Revisiting the conditional single signal model with phase uncertainty: application to time-delay estimation

Joan M. Bernabeu[a,b], Samuele Alteri[a,b,*], Antoine Blais[c], Lorenzo Ortega[d,b,a], Yoan Grégoire[e], Éric Chaumette[a]

[a] *ISAE-SUPAERO, University of Toulouse, 10 Av. Edouard Belin, 31400 Toulouse*
[b] *TéSA, 7, Boulevard de la Gare, 31500, Toulouse, France*
[c] *ENAC, University of Toulouse, 7 Av. Edouard Belin, 31400, Toulouse, France*
[d] *DR2I-IPSA, 81 Av. de Grande Bretagne, 31300 Toulouse, France*
[e] *CNES, 18 Av. Edouard Belin, 31400, Toulouse*

Abstract

Parameter estimation from phase-based observations arises in a wide range of applications, including navigation, radar, and communication systems. Within the conditional signal model, the received signal phase is typically represented as a single unknown term by merging hardware-induced and propagation-induced contributions into a complex amplitude, under the assumption that they are not independently identifiable. In this work, we revisit this modeling assumption and show, through an identifiability analysis, that hardware-induced and propagation-induced phase components are independently identifiable under suitable conditions. This result challenges the classical formulation and enables a more general signal model in which the phase structure is explicitly parameterized. Building on this formulation, we develop a general estimation framework for single-source parameter estimation, valid for an arbitrary parameter vector, and explicitly accounting for auxiliary phase observations affected by uncertainty. Within this framework, we derive Cramér–Rao bounds and maximum likelihood estimators (MLEs) for two scenarios: ideal hardware-phase compensation and a realistic case with noisy auxiliary phase measurements. We also implement a naive estimator that directly compensates the observed phase and applies MLE under ideal compensation. The proposed estimators are analyzed theoretically and validated through Monte Carlo simulations. The results show that phase uncertainty induces a performance limitation, leading to a saturation effect at high signal-to-noise ratios, whereas ideal phase compensation yields significant accuracy improvements over the conventional model. Finally, time-delay and Doppler estimation are considered to illustrate the proposed framework. The theoretical findings are validated using GPS L1 C/A and Kasami sequences, widely used in GNSS and communication systems.

Keywords: Cramér-Rao bound, carrier-phase, time-delay estimation, band-limited signals, phase uncertainty, maximum likelihood estimation

*Corresponding author
Email addresses: joan-miguel.bernabeu@isae-supaero.fr (Joan M. Bernabeu), samuele.alteri@isae-supaero.fr (Samuele Alteri), blais@enac.fr (Antoine Blais), lorenzo.ortega@ipsa.fr (Lorenzo Ortega), yoan.gregoire@cnes.fr (Yoan Grégoire), eric.chaumette@isae-supaero.fr (Éric Chaumette)

1. Introduction

Parameter estimation from phase-based observations is a fundamental problem in signal processing, with applications spanning satellite navigation [1, §2.1], radar systems [2, §1.4], and wireless communications [3, 4, 5]. In those systems, estimation performance is often critically driven by the structure of the received signal phase, which encodes both propagation-related information and hardware-dependent effects. Within the conditional signal model (CSM), the received signal phase is typically represented as a single unknown term by merging hardware-induced and propagation-induced contributions into a complex amplitude parameter [6, 7, 8]. That modeling choice simplifies the estimation problem and enables tractable performance analysis [9]. However, it implicitly assumes that those phase components are not independently identifiable, thereby discarding potentially exploitable structure in the signal. In this work, we show that this assumption is overly restrictive. Through a identifiability analysis, we prove that hardware-induced and propagation-induced phase components are independently identifiable under suitable signal conditions [10, 11, 12]. That result challenges the conventional formulation of the CSM and enables a more general signal model in which the phase structure is explicitly parameterized. Building on this result, we develop a general estimation framework for single-source parameter estimation, valid for an arbitrary parameter vector. The proposed framework explicitly incorporates auxiliary hardware-induced phase observations with associated uncertainty, as provided by practical calibration techniques [13, §17.6]. That allows us to quantify the impact of imperfect phase compensation and to characterize the regimes where phase-aware processing provides performance gains over conventional approaches. Within that framework, we derive both the maximum likelihood estimators (MLEs) and the Cramér–Rao bounds (CRB) in the general parameter setting. A naive estimator, directly using the external phase measurements without accounting for their uncertainty, is also considered. The analysis reveals a fundamental trade-off between signal-to-noise ratio (SNR) and phase uncertainty: while ideal phase compensation yields significant performance improvements, imperfect phase knowledge introduces a plateau in estimation accuracy, limiting performance at intermediate SNR levels [14, 15]. In that regime, both phase-aware and naive estimators converge to the same performance limit, showing that accounting for phase uncertainty does not provide performance gains. However, at higher SNR, the phase-aware estimator departs from that plateau and remains consistent with the theoretical bounds over an extended range, while the naive estimator remains constrained. At higher SNR, the proposed phase-aware estimator departs from this plateau and asymptotically recovers the classical CRB associated with the conventional model, where phase contributions are merged into a complex amplitude parameter. The main contributions of this paper are summarized as follows:

(i) We establish the independent identifiability of hardware-induced and propagation-induced phase components, challenging the conventional CSM.

(ii) We develop a general estimation framework and derive the corresponding MLEs and closed-form CRBs for arbitrary parameter vectors, explicitly accounting for auxiliary hardware-induced phase observations with uncertainty.

(iii) We provide a performance characterization by analyzing the asymptotic covariance, revealing the existence of SNR-dependent regimes and identifying when phase-aware processing yields gains over conventional approaches.

Finally, time-delay and Doppler estimation are considered as representative applications of the proposed framework, illustrating its practical relevance to ranging and synchronization problems [1]. The remainder of this paper is organized as follows: Section 2 introduces the CSM, providing the theoretical foundation for the study. Section 3 presents the identifiability analysis, while Section 4 and Section 5 derive the proposed estimator and the corresponding performance bounds, respectively. In Section 6, the asymptotic covariance matrix is derived to characterize the estimator's asymptotic behavior (large-sample and/or high SNR regime). The framework is then applied to time-delay estimation (TDE) scenarios in Section 7. Section 8 analyzes the ambiguity function, followed by an in-depth analysis of the cost function in Section 9. Finally, Section 10 presents simulation results to validate the theoretical findings, and Section 11 concludes the paper.

2. Conditional signal model

The CSM [12, 3] models deterministic signals observed in additive stochastic noise, where the signal amplitude is treated as an unknown deterministic parameter without any prior distribution, in contrast to the unconditional signal model (USM) which assumes a complex Gaussian prior. The CSM is frequently employed to model received signals in wireless communication and radar systems, accounting for various propagation phenomena that alter the signal's waveform as it traverses the transmission channel. These phenomena include path loss, multipath fading, angle-dependent array responses, Doppler shifts, etc. For a single source, the conventional model is

$$\mathbf{x} = \bar{\alpha}\bar{\mathbf{a}}(\boldsymbol{\eta}) + \mathbf{n}, \quad \mathbf{n} \sim \mathcal{CN}(0, \sigma_n^2 \mathbf{I}_N). \tag{1}$$

The complex gain $\bar{\alpha} \in \mathbb{C}$ jointly accounts for the overall unknown amplitude attenuation and unknown phase offset. The observation vector is denoted by $\mathbf{x} \in \mathbb{C}^N$, $\bar{\mathbf{a}}(\boldsymbol{\eta})$ is a known function of the parameter vector $\boldsymbol{\eta} \in \mathbb{R}^K$, collecting the parameters of interest (e.g., delay, Doppler, or angle-of-arrival parameters). The additive noise vector $\mathbf{n}$ is assumed to be circularly symmetric complex Gaussian. Thus, the parameter vector of the conventional Gaussian CSM is given by $\boldsymbol{\epsilon} = \begin{bmatrix}\sigma_n^2 & \mathrm{Re}\{\bar{\alpha}\} & \mathrm{Im}\{\bar{\alpha}\} & \boldsymbol{\eta}^T\end{bmatrix}^T$, where $\sigma_n^2 \in \mathbb{R}^+$ is the noise variance.

In the proposed formulation developed below, $\bar{\alpha} = \alpha e^{j\varphi}$, where $\alpha \in \mathbb{R}^+$ still accounts for the overall unknown amplitude attenuation, but $\varphi \in [-\pi, \pi)$ accounts for the phase terms non modeled by $\bar{\mathbf{a}}(\boldsymbol{\eta})$, including the hardware-induced phase offset. That parameterization decouples amplitude attenuation from phase effects, thereby enabling a dedicated analysis of phase calibration. The complete parameter vector is then defined as $\boldsymbol{\epsilon} = \begin{bmatrix}\sigma_n^2 & \alpha & \boldsymbol{\theta}^T\end{bmatrix}^T \in \mathbb{R}^{K+3}$, where $\boldsymbol{\theta} = \begin{bmatrix}\varphi & \boldsymbol{\eta}^T\end{bmatrix}^T \in \mathbb{R}^{K+1}$ are the parameters of interest. Let us also introduce $\boldsymbol{\zeta} = \begin{bmatrix}\alpha & \boldsymbol{\theta}^T\end{bmatrix}^T$.

The true (unknown) values of parameters are denoted $\bar{\alpha}^0 = \alpha^0 e^{j\varphi^0}$, $\boldsymbol{\eta}^0$, $\boldsymbol{\theta}^0$, $\boldsymbol{\zeta}^0$, $\boldsymbol{\epsilon}^0$.

2.1. CSM for signal transmission

Actually, a time-continuous model at the output of the Hilbert filter [16] is

$$x(t) = \alpha e^{j\varphi} a(t;\boldsymbol{\eta}) + n(t) = \alpha b(t;\boldsymbol{\theta}) + n(t), \quad n(t) \sim \mathcal{CN}(0, \sigma_n^2), \quad \boldsymbol{\theta} = [\varphi, \boldsymbol{\eta}^T]^T, \tag{2a}$$

where the channel-induced perturbations are parameterized by the vector $\boldsymbol{\eta}$, α and φ are global amplitude and phase factor primarily accounting for overall path loss and

other effects non-modeled by $a(t;\boldsymbol{\eta})$, such as transmitter and receiver miscalibration. Sampling the signal at the sampling frequency f_s yields the following alternative CSM, where N denotes the number of collected samples,

$$\left\{\begin{array}{lcl}\mathbf{x} & = & \alpha\mathbf{b}(\boldsymbol{\theta})+\mathbf{n},\quad \mathbf{n}\sim\mathcal{CN}\left(\mathbf{0},\sigma_n^2\mathbf{I}_N\right)\\ \mathbf{b}(\boldsymbol{\theta}) & = & \mathbf{a}(\boldsymbol{\eta})e^{j\varphi}\end{array}\right. ,\quad \alpha\in\mathbb{R}^+,\quad \boldsymbol{\theta}=\begin{bmatrix}\varphi\\ \boldsymbol{\eta}\end{bmatrix},\quad \varphi\in[-\pi,\pi]. \quad (2b)$$

The complete alternative vector of unknowns is defined as $\boldsymbol{\epsilon}=[\sigma_n^2,\alpha,\boldsymbol{\theta}^T]^T$. In many applications, such as in the TDE context, the transmission channel induces a phase depending on the transmission channel parameter vector $\boldsymbol{\eta}$, and the signal model (2b) becomes,

$$\left\{\begin{array}{lcl}\mathbf{x} & = & \alpha\mathbf{b}(\boldsymbol{\theta})+\mathbf{n},\quad \mathbf{n}\sim\mathcal{CN}\left(\mathbf{0},\sigma_n^2\mathbf{I}_N\right)\\ \mathbf{b}(\boldsymbol{\theta}) & = & \mathbf{a}(\boldsymbol{\eta})e^{j\varphi}\\ \mathbf{a}(\boldsymbol{\eta}) & = & \mathbf{c}(\boldsymbol{\eta})\odot\boldsymbol{e}^{j\boldsymbol{\psi}(\boldsymbol{\eta})}\end{array}\right. ,\quad \alpha\in\mathbb{R}^+,\quad \boldsymbol{\theta}=\begin{bmatrix}\varphi\\ \boldsymbol{\eta}\end{bmatrix},\quad \varphi\in[-\pi,\pi], \quad (3)$$

where $\odot$ denotes the Hadamard product and $\boldsymbol{e}^{j\boldsymbol{\psi}(\boldsymbol{\eta})}=\left[\ldots e^{j\psi\left(\frac{n}{f_s},\boldsymbol{\eta}\right)}\ldots\right]^T$, where $a(t;\boldsymbol{\eta})=c(t;\boldsymbol{\eta})e^{j\psi(t;\boldsymbol{\eta})}$. Here, the parameter vector is defined as $\boldsymbol{\eta}=\begin{bmatrix}\tau & \boldsymbol{\omega}^T\end{bmatrix}^T$, where τ denotes the time delay, while $\boldsymbol{\omega}$, if non empty, collects the remaining signal or propagation parameters, such as the Doppler frequency, the direction of arrival (DOA), or other application-dependent quantities. The quantities $(c(t;\boldsymbol{\eta}),\mathbf{c}(\boldsymbol{\eta}))$ denote the nominal received waveform after incorporating all propagation effects that do not induce a global phase shift and that are parameterized by $\boldsymbol{\eta}$. The factor $\left(e^{j\psi(t;\boldsymbol{\eta})},\boldsymbol{e}^{j\boldsymbol{\psi}(\boldsymbol{\eta})}\right)$ accounts for the phase contribution associated with the propagation parameters, yielding the waveform $(a(t;\boldsymbol{\eta}),\mathbf{a}(\boldsymbol{\eta}))$. The additional factor $e^{j\varphi}$ models the unknown hardware phase offset arising from transmitter and receiver imperfections, leading to the complete signal $(b(t;\boldsymbol{\theta}),\mathbf{b}(\boldsymbol{\theta}))$. That decomposition is introduced to explicitly separate the propagation-induced phase from the hardware-induced phase offset, which is the key aspect investigated in the subsequent estimation and performance analysis.
Thus, the main topic adressed by the paper is to analyse the contribution of the propagation-induced phase $\psi(\boldsymbol{\eta})$ to the estimation of $\boldsymbol{\eta}$ as a function of the a priori knowledge on φ.

2.1.1. Delay-Doppler case

When delay-Doppler effects are considered, the parameter vector $\boldsymbol{\eta}$ becomes $\boldsymbol{\eta}=[\tau,b]^{\mathrm{T}}$, where $b=v/c_e$ is the normalized Doppler factor, with v the relative speed between the transmitter and the receiver and c_e the speed of the light. If non empty, the vector $\boldsymbol{\omega}$ collects additional propagation-related parameters, such as direction-of-arrival (DOA) angles or other nuisance quantities. In this case, the propagation-induced phase $\boldsymbol{\psi}(\boldsymbol{\eta})$ (3) evolves over time as

$$e^{j\psi(t;\boldsymbol{\eta})}=e^{-j2\pi f_c(\tau+b(t-\tau))}, \quad (4a)$$

$$c(t;\boldsymbol{\eta})=c((1-b)(t-\tau))\approx c(t-\tau), \quad (4b)$$

where (4a) accounts for both the propagation delay and the Doppler-induced time scaling. The general expression of $\mathbf{c}(\boldsymbol{\eta})$ depends on the adopted channel model. In the delay–Doppler scenario, under the narrowband assumption, the received baseband signal is represented by (4b), where the Doppler effect manifests itself as a temporal

compression or dilation of the transmitted waveform.

2.1.2. Delay-only assumption

In many practical scenarios, Doppler effects can be neglected, leading to the simplified model with parameter vector $\eta = \tau$ and propagation-induced phase

$$e^{-j2\pi f_c \tau} = e^{j\psi(t;\eta)}, \tag{5a}$$

$$c(t;\eta) \approx c(t-\tau). \tag{5b}$$

2.2. CSM with auxiliary phase observables

The identifiability analysis (Section 3) shows that the hardware-induced phase φ and the propagation-induced phase $\psi(\boldsymbol{\eta})$ can be treated as independent parameters. In practice, partial information about φ is often available through calibration or tracking loops, although affected by uncertainty. To model that, we introduce a noisy auxiliary observation x_a of φ with a known (from a calibration process) variance $\sigma_{n_a}^2$,

$$\begin{cases} \mathbf{x} &= \alpha\left(\mathbf{c}(\boldsymbol{\eta}) \odot \boldsymbol{e}^{j\boldsymbol{\psi}(\boldsymbol{\eta})}\right) e^{j\varphi} + \mathbf{n}, & \mathbf{n} \sim \mathcal{CN}\left(\mathbf{0}, \sigma_n^2 \mathbf{I}_N\right) \\ x_a &= \varphi + n_a, & n_a \sim \mathcal{N}\left(0, \sigma_{n_a}^2\right) \end{cases}, \ \alpha \in \mathbb{R}^+, \ \boldsymbol{\theta} = \begin{bmatrix} \varphi \\ \boldsymbol{\eta} \end{bmatrix}, \ \varphi \in [-\pi, \pi]. \tag{6}$$

The Gaussian approximation for x_a is valid when $3\sigma_{n_a} \ll \pi$, ensuring negligible phase wrapping. The joint probability density function factorizes as

$$P(\mathbf{x}, x_a; \boldsymbol{\epsilon}) = P(\mathbf{x}; \boldsymbol{\epsilon}) P(x_a; \varphi). \tag{7}$$

In contrast, conventional approaches based on the model in (1) [6] merge any scalar factor of propagation-induced phase $\boldsymbol{\psi}(\boldsymbol{\eta})$ (e.g. $2\pi f_c \tau$ (4a)(5a)) and the hardware phase offset φ into a single complex gain $\bar{\alpha}$. Although that representation is mathematically suitable, it obscures the physical origin of the individual phase contributions and therefore precludes their separate estimation and calibration.

3. Parameter identifiability

Parameter identifiability characterizes whether distinct parameter values produce distinct probability distributions of the observed data. Formally, the parameter vector $\boldsymbol{\epsilon}$ is identifiable if

$$P(\mathbf{x}; \boldsymbol{\epsilon}_1) = P(\mathbf{x}; \boldsymbol{\epsilon}_2) \ \Rightarrow \ \boldsymbol{\epsilon}_1 = \boldsymbol{\epsilon}_2. \tag{8}$$

For the Gaussian CSM, identifiability reduces to the injectivity of the mapping $(\alpha, \boldsymbol{\theta}) \mapsto \alpha \mathbf{b}(\boldsymbol{\theta})$, since the noise variance is trivially identifiable. Equality of the likelihood functions implies

$$\alpha_1 \mathbf{b}(\boldsymbol{\theta}_1) = \alpha_2 \mathbf{b}(\boldsymbol{\theta}_2). \tag{9}$$

This equality holds if and only if there exists a complex scalar $\lambda \in \mathbb{C}$ such that

$$\mathbf{b}(\boldsymbol{\theta}_1) = \lambda \mathbf{b}(\boldsymbol{\theta}_2), \tag{10}$$

i.e., the two vectors are collinear. Therefore, non-identifiability arises when distinct parameter values produce collinear signal vectors. A sufficient condition for identifiability is thus

$$\left|\mathbf{b}(\boldsymbol{\theta}_1)^H \mathbf{b}(\boldsymbol{\theta}_2)\right| < \|\mathbf{b}(\boldsymbol{\theta}_1)\| \, \|\mathbf{b}(\boldsymbol{\theta}_2)\|, \quad \forall \boldsymbol{\theta}_1 \neq \boldsymbol{\theta}_2, \tag{11}$$

which ensures that no two distinct parameter values yield collinear signal vectors. The restriction $\alpha \in \mathbb{R}^+$ in (2b) is essential to remove phase ambiguity. If $\alpha \in \mathbb{C}$, the model is invariant under the transformation $(\alpha, \varphi) \mapsto (\alpha e^{j\delta}, \varphi - \delta)$ for any $\delta \in \mathbb{R}$, leading to infinitely many equivalent parameterizations. By constraining α to be real and positive, that ambiguity is eliminated, enabling the independent identification of phase components in $\boldsymbol{\theta}$. For the signal model $\mathbf{b}(\boldsymbol{\theta}) = \mathbf{a}(\boldsymbol{\eta})e^{j\varphi}$, condition (11) reduces to

$$\left|\mathbf{a}(\boldsymbol{\eta}_1)^H \mathbf{a}(\boldsymbol{\eta}_2)\right| < \|\mathbf{a}(\boldsymbol{\eta}_1)\| \, \|\mathbf{a}(\boldsymbol{\eta}_2)\|, \quad \forall \boldsymbol{\eta}_1 \neq \boldsymbol{\eta}_2. \tag{12}$$

Moreover, when $\alpha \in \mathbb{R}^+$, the complex scalar λ reduces to a pure phase term. Consequently, φ is identifiable modulo 2π, i.e., $\varphi_1 \equiv \varphi_2 \pmod{2\pi}$. By restricting $\varphi \in [-\pi, \pi)$, a unique representative is selected, so that both $\boldsymbol{\eta}$ and φ are uniquely identified within the adopted parameterization. That result shows that the hardware-induced phase φ can be separated from the propagation-induced phase $\psi(\boldsymbol{\eta})$ in (3), provided that condition (12) holds and that the amplitude is constrained to $\alpha \in \mathbb{R}^+$. This challenges the conventional modeling assumption in which the hardware-induced phase and the propagation-induced phase are absorbed into a single complex amplitude.

It should be noted that this identifiability result is established under the assumed single-source conditional signal model. In particular, it assumes that the received signal is described by a single propagation path and that no additional nuisance parameters, such as multipath components or unmodeled residual calibration biases, are present. Such effects fall outside the scope of the present model and may compromise identifiability analysis, unless they are explicitly incorporated into the signal model.

4. Maximum-Likelihood Estimator

This section develops the phase-aware estimator for the extended signal model in equation (6) that incorporates auxiliary phase observables. First, the constrained maximum likelihood framework is presented, which establishes the cost function through elimination of nuisance parameters. From that framework, two practical implementations emerge: a) the naive estimator, which directly applies phase measurements without statistical consideration to mitigate the phase error, and b) what we refer to as the phase-aware estimator, which explicitly accounts for the phase measurement uncertainty $\sigma_{n_a}^2$ through polynomial optimization. This formulation enables assessment of the operating conditions under which the improved estimation performance of the phase-aware approach justifies its additional computational cost.

4.1. Constrained Maximum Likelihood Framework

To derive the phase-aware estimator, the joint probability density function in equation (7) serves as the starting point. The negative log-likelihood cost function is equivalent to

$$\mathcal{S}_0(\mathbf{x}, x_a; \boldsymbol{\epsilon}) = \frac{\|\mathbf{x} - \mathbf{a}(\boldsymbol{\eta})e^{j\varphi}\alpha\|^2}{\sigma_n^2} + N\ln(\pi\sigma_n^2) + \frac{(x_a - \varphi)^2}{2\sigma_{n_a}^2}, \tag{13}$$

since $\sigma_{n_a}^2$ is known. Firstly, for the sake of simplicity, let us assume that σ_n^2 is known as well (i.e., has been calibrated as well). Then $\mathcal{S}_0$ simplifies to

$$\mathcal{S}_1(\mathbf{x}, x_a; \boldsymbol{\zeta}) = \frac{\|\mathbf{x} - \mathbf{a}(\boldsymbol{\eta})e^{j\varphi}\alpha\|^2}{\sigma_n^2} + \frac{(x_a - \varphi)^2}{2\sigma_{n_a}^2}.$$

where $\boldsymbol{\zeta} = \begin{bmatrix}\alpha & \boldsymbol{\theta}^T\end{bmatrix}^T$, with $\alpha \in \mathbb{R}^+$ denoting the unknown signal amplitude and $\boldsymbol{\theta}$ collecting the remaining parameters of interest. Since α is a nuisance parameter, it is eliminated by replacing it with its maximum likelihood (ML) estimate. To facilitate the derivation, the complex signal model is expressed in real-valued equivalent form

$$\underline{\mathbf{x}} = \begin{bmatrix}\mathrm{Re}\{\mathbf{x}\} \\ \mathrm{Im}\{\mathbf{x}\}\end{bmatrix} \in \mathbb{R}^{2N}, \quad \underline{\mathbf{a}}(\boldsymbol{\eta}) = \begin{bmatrix}\mathrm{Re}\{\mathbf{a}(\boldsymbol{\eta})e^{j\varphi}\} \\ \mathrm{Im}\{\mathbf{a}(\boldsymbol{\eta})e^{j\varphi}\}\end{bmatrix} \in \mathbb{R}^{2N}, \tag{14}$$

noting that $\|\mathbf{x} - \mathbf{a}(\boldsymbol{\eta})e^{j\varphi}\alpha\|^2 = \|\underline{\mathbf{x}} - \underline{\mathbf{a}}(\boldsymbol{\eta})\alpha\|^2$. Therefore, $\left(\widehat{\boldsymbol{\theta}}, \widehat{\alpha}\right) = \arg\min_{\boldsymbol{\theta}, \alpha \in \mathbb{R}^+}\{\|\underline{\mathbf{x}} - \underline{\mathbf{a}}(\boldsymbol{\eta})\alpha\|^2\}$, where

$$\|\underline{\mathbf{x}} - \underline{\mathbf{a}}(\boldsymbol{\eta})\alpha\|^2 = \|\boldsymbol{\Pi}_{\underline{\mathbf{a}}(\boldsymbol{\eta})}(\underline{\mathbf{x}} - \underline{\mathbf{a}}(\boldsymbol{\eta})\alpha)\|^2 + \|\boldsymbol{\Pi}^{\perp}_{\underline{\mathbf{a}}(\boldsymbol{\eta})}\underline{\mathbf{x}}\|^2. \tag{15}$$

Expanding the first term yields

$$\|\boldsymbol{\Pi}_{\underline{\mathbf{a}}(\boldsymbol{\eta})}(\underline{\mathbf{x}} - \underline{\mathbf{a}}(\boldsymbol{\eta})\alpha)\|^2 = \|\underline{\mathbf{a}}(\boldsymbol{\eta})\|^2 \left(\widehat{\alpha}_u(\boldsymbol{\eta}) - \alpha\right)^2, \tag{16}$$

where the unconstrained amplitude estimate is

$$\widehat{\alpha}_u(\boldsymbol{\eta}) = \frac{\underline{\mathbf{a}}(\boldsymbol{\eta})^T\underline{\mathbf{x}}}{\underline{\mathbf{a}}(\boldsymbol{\eta})^T\underline{\mathbf{a}}(\boldsymbol{\eta})} = \frac{\mathrm{Re}\{e^{-j\varphi}\mathbf{a}(\boldsymbol{\eta})^H\mathbf{x}\}}{\|\mathbf{a}(\boldsymbol{\eta})\|^2}. \tag{17}$$

Under the constraint $\alpha \in \mathbb{R}^+$ and assuming that the signal is present, i.e. $\widehat{\alpha}_u(\boldsymbol{\eta}) > 0$, which corresponds to $\mathrm{Re}\{e^{-j\varphi}\mathbf{a}(\boldsymbol{\eta})^H\mathbf{x}\} > 0$, the optimal amplitude estimate is $\widehat{\alpha} = \widehat{\alpha}_u(\boldsymbol{\eta})$. Substituting this eliminates the first term, reducing the cost function $\mathcal{S}_1$ to

$$\mathcal{S}_2(\mathbf{x}, x_a; \boldsymbol{\eta}, \varphi) = \mathcal{S}_1(\mathbf{x}, x_a; \widehat{\alpha}, \boldsymbol{\eta}, \varphi) = \frac{\|\boldsymbol{\Pi}^{\perp}_{\underline{\mathbf{a}}(\boldsymbol{\eta})}\underline{\mathbf{x}}\|^2}{\sigma_n^2} + \frac{(x_a - \varphi)^2}{2\sigma_{n_a}^2} = \frac{\|\underline{\mathbf{x}}\|^2}{\sigma_n^2} - \frac{\|\boldsymbol{\Pi}_{\underline{\mathbf{a}}(\boldsymbol{\eta})}\underline{\mathbf{x}}\|^2}{\sigma_n^2} + \frac{(x_a - \varphi)^2}{2\sigma_{n_a}^2}. \tag{18}$$

Since $\|\underline{\mathbf{x}}\|^2$ is constant, using the relationship $\underline{\mathbf{a}}(\boldsymbol{\eta})^T\underline{\mathbf{x}} = \mathrm{Re}\{\left(\mathbf{a}(\boldsymbol{\eta})e^{j\varphi}\right)^H\mathbf{x}\}$, the cost function simplifies to

$$\mathcal{S}_2(\mathbf{x}, x_a; \boldsymbol{\eta}, \varphi) = \frac{\sigma_n^2}{2\sigma_{n_a}^2}(x_a - \varphi)^2 - \mathrm{Re}\left\{e^{-j\varphi}\frac{\mathbf{a}(\boldsymbol{\eta})^H\mathbf{x}}{\|\mathbf{a}(\boldsymbol{\eta})\|}\right\}^2, \tag{19}$$

with the constraint $\mathrm{Re}\{e^{-j\varphi}\mathbf{a}(\boldsymbol{\eta})^H\mathbf{x}\} > 0$ ensuring $\widehat{\alpha} > 0$. By factoring out the phase compensation through x_a,

$$\mathcal{S}_2(\mathbf{x}, x_a; \boldsymbol{\eta}, \varphi) = \frac{\sigma_n^2}{2\sigma_{n_a}^2}(x_a - \varphi)^2 - \mathrm{Re}\left\{e^{j(x_a - \varphi)}\gamma(\boldsymbol{\eta})\right\}^2, \tag{20}$$

where $\gamma(\boldsymbol{\eta})$ is defined as the normalized "naive" correlation function (see also (23))

$$\gamma(\boldsymbol{\eta}) = \frac{\mathbf{a}(\boldsymbol{\eta})^H(e^{-jx_a}\mathbf{x})}{\|\mathbf{a}(\boldsymbol{\eta})\|}. \tag{21}$$

Introducing the phase compensation error $\varepsilon = \varphi - x_a$ transforms the cost function to

$$\mathcal{S}_2(\mathbf{x}, x_a; \boldsymbol{\eta}, \varepsilon) = \frac{\sigma_n^2}{2\sigma_{n_a}^2}\varepsilon^2 - \mathrm{Re}\left\{e^{-j\varepsilon}\gamma(\boldsymbol{\eta})\right\}^2. \tag{22}$$

This formulation reveals the fundamental structure: the estimation problem requires jointly optimizing over both the phase error ε and the parameters of interest $\boldsymbol{\eta}$.

4.2. Naive Estimator

The naive approach emerges when the available phase observable x_a is directly applied for compensation without consideration of its measurement uncertainty. This corresponds to set $\varepsilon = 0$ in the cost function (22) despite the presence of noise n_a in the phase measurement, yielding

$$\widehat{\boldsymbol{\eta}_n} = \underset{\{\boldsymbol{\eta}|\mathrm{Re}\{\gamma(\boldsymbol{\eta})\}>0\}}{\arg\max} \left\{\mathrm{Re}\left\{\gamma(\boldsymbol{\eta})\right\}^2\right\}, \tag{23}$$

where $\gamma(\boldsymbol{\eta})$ represents thus the normalized naive correlation function (21). That estimator provides a computationally efficient implementation applicable whenever auxiliary phase measurements are available and serves as a practical benchmark of estimation performance under phase compensation without sophisticated statistical processing. Its performance relative to the phase-aware estimator quantifies the benefit of accurately characterizing uncertainty.

4.3. Phase-Aware Estimator

The proposed phase-aware estimator explicitly incorporates the uncertainty associated with the phase measurement, characterized by the variance $\sigma_{n_a}^2$. To account for that uncertainty, the optimization jointly considers both the residual phase ε and the parameter vector $\boldsymbol{\eta}$. However, a direct joint optimization would be computationally prohibitive. To mitigate this complexity, the cost function term in (22) is reformulated by exploiting the identity $\mathrm{Re}\{z\}^2 = \frac{\mathrm{Re}\{z^2\}+|z|^2}{2}$, valid for any complex number z, leading to

$$\mathrm{Re}\left\{e^{-j\varepsilon}\gamma(\boldsymbol{\eta})\right\}^2 = \frac{\mathrm{Re}\left\{e^{-j2\varepsilon}\gamma(\boldsymbol{\eta})^2\right\} + |\gamma(\boldsymbol{\eta})|^2}{2}. \tag{24}$$

Within the asymptotic regime where $\sigma_{n_a}^2 \ll (\frac{\pi}{3})^2$ implies $\varepsilon \ll 1$, the exponential term $e^{-j2\varepsilon}$ can be expanded using a high-order Taylor series. A seventh-order expansion is adopted to accurately characterize the estimator behavior,

$$e^{-j2\varepsilon} \simeq 1 - 2\varepsilon^2 + \frac{2}{3}\varepsilon^4 - \frac{4}{45}\varepsilon^6 - j\left(2\varepsilon - \frac{4}{3}\varepsilon^3 + \frac{4}{15}\varepsilon^5 - \frac{8}{315}\varepsilon^7\right). \tag{25}$$

The computation of the asymptotic covariance matrix confirms the convergence of the estimator. Although a fifth-order expansion already provides a valid asymptotic characterization, using a seventh-order expansion ensures higher numerical accuracy and yields a more precise approximation in the high-SNR regime. Those errors may give the misleading impression of a secondary plateau (Section 7). The seventh-order expansion, on the other hand, represents the lowest-order truncation that preserves asymptotic consistency and avoids such high-SNR artifacts. Although that behavior might initially appear to stem from the phase uncertainty $\sigma_{n_a}^2$, the covariance analysis presented in Section 6 confirms that it originates from limitations of the polynomial

approximation. By substituting the seventh-order expansion in (24), one obtains

$$\mathrm{Re}\{e^{-j\varepsilon}\gamma(\boldsymbol{\eta})\}^2 \simeq -\frac{4}{315}\mathrm{Im}\{\gamma(\boldsymbol{\eta})^2\}\,\varepsilon^7 - \frac{2}{45}\mathrm{Re}\{\gamma(\boldsymbol{\eta})^2\}\,\varepsilon^6 + \frac{2}{15}\mathrm{Im}\{\gamma(\boldsymbol{\eta})^2\}\,\varepsilon^5$$
$$+\frac{1}{3}\mathrm{Re}\{\gamma(\boldsymbol{\eta})^2\}\,\varepsilon^4 - \frac{2}{3}\mathrm{Im}\{\gamma(\boldsymbol{\eta})^2\}\,\varepsilon^3 - \mathrm{Re}\{\gamma(\boldsymbol{\eta})^2\}\,\varepsilon^2 + \mathrm{Im}\{\gamma(\boldsymbol{\eta})^2\}\,\varepsilon + \mathrm{Re}\{\gamma(\boldsymbol{\eta})\}^2, \quad (26)$$

where $\mathrm{Im}\{\cdot\}$ denotes the imaginary part operator. Incorporating this expression into the cost function yields

$$\mathcal{S}_2(\mathbf{x};\boldsymbol{\theta}) \simeq \frac{4}{315}\mathrm{Im}\{\gamma(\boldsymbol{\eta})^2\}\,\varepsilon^7 + \frac{2}{45}\mathrm{Re}\{\gamma(\boldsymbol{\eta})^2\}\,\varepsilon^6 - \frac{2}{15}\mathrm{Im}\{\gamma(\boldsymbol{\eta})^2\}\,\varepsilon^5$$
$$-\frac{1}{3}\mathrm{Re}\{\gamma(\boldsymbol{\eta})^2\}\,\varepsilon^4+\frac{2}{3}\mathrm{Im}\{\gamma(\boldsymbol{\eta})^2\}\,\varepsilon^3+\frac{1}{2}\left(\frac{\sigma_n^2}{\sigma_{n_a}^2} + 2\mathrm{Re}\{\gamma(\boldsymbol{\eta})^2\}\right)\varepsilon^2-\mathrm{Im}\{\gamma(\boldsymbol{\eta})^2\}\,\varepsilon-\mathrm{Re}\{\gamma(\boldsymbol{\eta})\}^2. \quad (27)$$

The resulting polynomial form enables a two-stage estimation strategy. First, the phase error ε is estimated for a given $\boldsymbol{\eta}$ as

$$\widehat{\varepsilon}(\boldsymbol{\eta}) = \underset{\{\varepsilon\,|\,\mathrm{Re}\{e^{-j\varepsilon}\gamma(\boldsymbol{\eta})\}>0\}}{\arg}\left\{\frac{\partial\mathcal{S}_2(\mathbf{x},x_a;\boldsymbol{\eta},\varepsilon)}{\partial\varepsilon} = 0\right\}, \quad (28)$$

which requires solving the sixth-degree polynomial

$$\frac{\partial\mathcal{S}_2(\mathbf{x},x_a;\boldsymbol{\eta},\varepsilon)}{\partial\varepsilon} \simeq \frac{4}{45}\mathrm{Im}\{\gamma(\boldsymbol{\eta})^2\}\,\varepsilon^6 + \frac{4}{15}\mathrm{Re}\{\gamma(\boldsymbol{\eta})^2\}\,\varepsilon^5 - \frac{2}{3}\mathrm{Im}\{\gamma(\boldsymbol{\eta})^2\}\,\varepsilon^4$$
$$-\frac{4}{3}\mathrm{Re}\{\gamma(\boldsymbol{\eta})^2\}\,\varepsilon^3 + 2\mathrm{Im}\{\gamma(\boldsymbol{\eta})^2\}\,\varepsilon^2 +\left(\frac{\sigma_n^2}{\sigma_{n_a}^2} + 2\mathrm{Re}\{\gamma(\boldsymbol{\eta})^2\}\right)\varepsilon - \mathrm{Im}\{\gamma(\boldsymbol{\eta})^2\}. \quad (29)$$

Among the six polynomial roots, some may be complex. Since ε is real-valued, only the real part of each candidate is considered. The estimate is then obtained as

$$\widehat{\varepsilon} = \arg\min\left\{\mathcal{S}_2(\mathbf{x},x_a;\boldsymbol{\eta},\mathrm{Re}\{\widehat{\varepsilon}_1\}),\ldots,\mathcal{S}_2(\mathbf{x},x_a;\boldsymbol{\eta},\mathrm{Re}\{\widehat{\varepsilon}_6\})\right\}. \quad (30)$$

Once $\widehat{\varepsilon}$ is obtained for each candidate $\boldsymbol{\eta}$, the phase-aware estimator is expressed as

$$\widehat{\boldsymbol{\eta}} = \arg\min_{\boldsymbol{\eta}}\{\mathcal{S}_2(\mathbf{x},x_a;\boldsymbol{\eta},\widehat{\varepsilon}(\boldsymbol{\eta}))\} = \arg\min_{\boldsymbol{\eta}}\left\{\frac{\sigma_n^2\widehat{\varepsilon}(\boldsymbol{\eta})^2}{2\sigma_{n_a}^2} - \mathrm{Re}\left\{e^{-j\,\widehat{\varepsilon}(\boldsymbol{\eta})}\gamma(\boldsymbol{\eta})\right\}^2\right\}. \quad (31)$$

That phase-aware formulation effectively bridges analytical tractability and statistical rigor by embedding the variance $\sigma_{n_a}^2$ within the polynomial coefficients. Then, the estimator remains consistent under non-negligible phase uncertainty while avoiding the computational cost of full joint optimization. In the delay–Doppler case, the minimization in (31) is implemented through a two-dimensional grid search over the delay and normalized Doppler parameters, i.e., over (τ, b).

4.4. Unknown noise power

If the noise power is unknown, the negative log-likelihood cost function reads

$$\mathcal{S}_0(\mathbf{x}, x_a; \boldsymbol{\epsilon}) = \frac{\|\mathbf{x} - \mathbf{a}(\boldsymbol{\eta})e^{j\varphi}\alpha\|^2}{\sigma_n^2} + N\ln(\pi\sigma_n^2) + \frac{(x_a - \varphi)^2}{2\sigma_{n_a}^2}, \tag{32}$$

and the nuisance parameters σ_n^2 must be eliminated through its maximum likelihood estimate,

$$\widehat{\sigma_n^2} = \frac{\|\mathbf{x} - \mathbf{a}(\boldsymbol{\eta})e^{j\varphi}\alpha\|^2}{N}. \tag{33}$$

Substituting this estimate back into S_0 produces

$$\mathcal{S}_1(\mathbf{x}, x_a; \boldsymbol{\zeta}) = N\ln\left(\|\mathbf{x} - \mathbf{a}(\boldsymbol{\eta})e^{j\varphi}\alpha\|^2\right) + \frac{(x_a - \varphi)^2}{2\sigma_{n_a}^2}, \tag{34}$$

and (22) becomes

$$\mathcal{S}_2(\mathbf{x}, x_a; \boldsymbol{\eta}, \varepsilon) = \frac{\varepsilon^2}{2\sigma_{n_a}^2} + N\log\left(\|\mathbf{x}\|^2 - \mathrm{Re}\left\{e^{-j\varepsilon}\gamma(\boldsymbol{\eta})\right\}^2\right). \tag{35}$$

Then, as above, the phase error $\boldsymbol{\varepsilon}$ is estimated for a given $\boldsymbol{\eta}$ as

$$\widehat{\varepsilon}(\boldsymbol{\eta}) = \underset{\{\varepsilon \,|\, \mathrm{Re}\{e^{-j\varepsilon}\gamma(\boldsymbol{\eta})\}>0\}}{\arg} \left\{\frac{\partial \mathcal{S}_2(\mathbf{x}, x_a; \boldsymbol{\eta}, \varepsilon)}{\partial \varepsilon} = 0\right\}, \tag{36}$$

by resorting to a seventh-order expansion of $e^{-j2\varepsilon}$ (25) and $\mathrm{Re}\left\{e^{-j\varepsilon}\gamma(\boldsymbol{\eta})\right\}^2$ (26) which requires solving an eigth-degree (instead of sixth-degree (29)) polynomial.

5. Cramér-Rao Bound

The extended signal model incorporating phase observables modifies the structure of the FIM, enabling quantification of performance improvements as a function of phase observation quality. This section derives the CRB for the extended CSM (6), establishing fundamental performance limits that account for the information content of auxiliary phase measurements. The joint probability density function in equation (7) leads to a FIM with a block structure reflecting the separation between signal and phase observations, which decomposes as,

$$\begin{aligned}\mathbf{F}_{\boldsymbol{\epsilon}} &= E\left\{-\frac{\partial^2 \ln(P(\mathbf{x}, x_a; \boldsymbol{\epsilon}))}{\partial\boldsymbol{\epsilon}\partial\boldsymbol{\epsilon}^T}\right\} = E\left\{-\frac{\partial^2\big(\ln P(\mathbf{x}; \boldsymbol{\epsilon}) + \ln P(x_a; \varphi)\big)}{\partial\boldsymbol{\epsilon}\partial\boldsymbol{\epsilon}^T}\right\}, \\ &= E\left\{-\frac{\partial^2 \ln P(\mathbf{x}; \boldsymbol{\epsilon})}{\partial\boldsymbol{\epsilon}\partial\boldsymbol{\epsilon}^T}\right\} + E\left\{-\frac{\partial^2 \ln P(x_a; \varphi))}{\partial\boldsymbol{\epsilon}\partial\boldsymbol{\epsilon}^T}\right\} = \mathbf{F}(\mathbf{x}, \boldsymbol{\epsilon}) + \mathbf{F}(\varphi),\end{aligned} \tag{37}$$

where $\mathbf{F}(\mathbf{x}, \boldsymbol{\epsilon})$ corresponds to the information contribution from the complex baseband signal observation, and $\mathbf{F}(\varphi)$ accounts for the real-valued information from the noisy phase measurement. $\mathbf{F}(\boldsymbol{\epsilon})$ is then obtained by direct application of the Slepian-Bangs Formula (SBF) [17], revealing a blocks structure organized according to the parameters

of interest as,

$$\mathbf{F}_{\boldsymbol{\epsilon}} = \begin{bmatrix} \frac{N}{(\sigma_n^2)^2} & \mathbf{0}^T \\ \mathbf{0} & \mathbf{F}_{\boldsymbol{\zeta}|\boldsymbol{\epsilon}} \end{bmatrix}, \quad \mathbf{F}_{\boldsymbol{\zeta}|\boldsymbol{\epsilon}} = \begin{bmatrix} F_{\alpha|\boldsymbol{\epsilon}} & \mathbf{F}_{\alpha,\boldsymbol{\theta}|\boldsymbol{\epsilon}} \\ \mathbf{F}_{\boldsymbol{\theta},\alpha|\boldsymbol{\epsilon}} & \mathbf{F}_{\boldsymbol{\theta}|\boldsymbol{\epsilon}} \end{bmatrix}, \quad \mathbf{F}_{\boldsymbol{\theta}|\boldsymbol{\epsilon}} = \begin{bmatrix} F_{\varphi|\boldsymbol{\epsilon}} & \mathbf{F}_{\varphi,\boldsymbol{\eta}|\boldsymbol{\epsilon}} \\ \mathbf{F}_{\boldsymbol{\eta},\varphi|\boldsymbol{\epsilon}} & \mathbf{F}_{\boldsymbol{\eta}|\boldsymbol{\epsilon}} \end{bmatrix}, \tag{38a}$$

with,

$$\mathbf{F}_{\boldsymbol{\zeta}|\boldsymbol{\epsilon}} = \begin{bmatrix} \frac{2}{\sigma_n^2}\|\mathbf{a}(\boldsymbol{\eta})\|^2 & \left[0, \quad \frac{2\alpha}{\sigma_n^2}\mathrm{Re}\left\{\mathbf{a}(\boldsymbol{\eta})^H \frac{\partial \mathbf{a}(\boldsymbol{\eta})}{\partial \boldsymbol{\eta}^T}\right\}\right] \\ \left[0, \quad \frac{2\alpha}{\sigma_n^2}\mathrm{Re}\left\{\mathbf{a}(\boldsymbol{\eta})^H \frac{\partial \mathbf{a}(\boldsymbol{\eta})}{\partial \boldsymbol{\eta}^T}\right\}\right]^T & \mathbf{F}_{\boldsymbol{\theta}|\boldsymbol{\epsilon}} \end{bmatrix}, \tag{38b}$$

$$\mathbf{F}_{\boldsymbol{\theta}|\boldsymbol{\epsilon}} = \frac{2\alpha^2}{\sigma_n^2}\begin{bmatrix} \|\mathbf{a}(\boldsymbol{\eta})\|^2 + \frac{\sigma_n^2}{2\alpha^2\sigma_{n_a}^2} & \mathrm{Im}\left\{\mathbf{a}(\boldsymbol{\eta})^H \frac{\partial \mathbf{a}(\boldsymbol{\eta})}{\partial \boldsymbol{\eta}^T}\right\} \\ \mathrm{Im}\left\{\mathbf{a}(\boldsymbol{\eta})^H \frac{\partial \mathbf{a}(\boldsymbol{\eta})}{\partial \boldsymbol{\eta}^T}\right\}^T & \mathrm{Re}\left\{\left(\frac{\partial \mathbf{a}(\boldsymbol{\eta})}{\partial \boldsymbol{\eta}^T}\right)^H \frac{\partial \mathbf{a}(\boldsymbol{\eta})}{\partial \boldsymbol{\eta}^T}\right\} \end{bmatrix}. \tag{38c}$$

In the top-left element of (38c), the additive term $\frac{\sigma_n^2}{2\sigma_{n_a}^2}$ reflects the information contributed by the noisy measurement of φ. The CRB is directly obtained by inverting $\mathbf{F}_{\boldsymbol{\zeta}|\boldsymbol{\epsilon}}$, by blocks [18, §15],

$$\begin{aligned} \mathbf{CRB}_{\boldsymbol{\theta}|\boldsymbol{\epsilon}} &= \left(\mathbf{F}_{\boldsymbol{\theta}|\boldsymbol{\epsilon}} - \mathbf{F}_{\boldsymbol{\theta},\alpha|\boldsymbol{\epsilon}}\mathbf{F}_{\alpha|\boldsymbol{\epsilon}}^{-1}\mathbf{F}_{\alpha,\boldsymbol{\theta}|\boldsymbol{\epsilon}}\right)^{-1}, \\ &= \left(\mathbf{F}_{\boldsymbol{\theta}|\boldsymbol{\epsilon}} - \frac{\left[0, \quad \frac{2\alpha}{\sigma_n^2}\mathrm{Re}\left\{\mathbf{a}(\boldsymbol{\eta})^H \frac{\partial \mathbf{a}(\boldsymbol{\eta})}{\partial \boldsymbol{\eta}^T}\right\}\right]^T \left[0, \quad \frac{2\alpha}{\sigma_n^2}\mathrm{Re}\left\{\mathbf{a}(\boldsymbol{\eta})^H \frac{\partial \mathbf{a}(\boldsymbol{\eta})}{\partial \boldsymbol{\eta}^T}\right\}\right]}{\frac{2}{\sigma_n^2}\|\mathbf{a}(\boldsymbol{\eta})\|^2}\right)^{-1}, \\ &= \frac{\sigma_n^2}{2\alpha^2}\begin{bmatrix} \|\mathbf{a}(\boldsymbol{\eta})\|^2 + \frac{\sigma_n^2}{2\alpha^2\sigma_{n_a}^2} & \mathrm{Im}\left\{\mathbf{a}(\boldsymbol{\eta})^H \frac{\partial \mathbf{a}(\boldsymbol{\eta})}{\partial \boldsymbol{\eta}^T}\right\} \\ \mathrm{Im}\left\{\mathbf{a}(\boldsymbol{\eta})^H \frac{\partial \mathbf{a}(\boldsymbol{\eta})}{\partial \boldsymbol{\eta}^T}\right\}^T & \boldsymbol{\Phi}_{\boldsymbol{\eta}|\boldsymbol{\epsilon}} \end{bmatrix}^{-1}, \end{aligned} \tag{39}$$

where,

$$\boldsymbol{\Phi}_{\boldsymbol{\eta}|\boldsymbol{\epsilon}} = \mathrm{Re}\left\{\left(\frac{\partial \mathbf{a}(\boldsymbol{\eta})}{\partial \boldsymbol{\eta}^T}\right)^H \frac{\partial \mathbf{a}(\boldsymbol{\eta})}{\partial \boldsymbol{\eta}^T}\right\} - \frac{\mathrm{Re}\left\{\mathbf{a}(\boldsymbol{\eta})^H \frac{\partial \mathbf{a}(\boldsymbol{\eta})}{\partial \boldsymbol{\eta}^T}\right\}^T \mathrm{Re}\left\{\mathbf{a}(\boldsymbol{\eta})^H \frac{\partial \mathbf{a}(\boldsymbol{\eta})}{\partial \boldsymbol{\eta}^T}\right\}}{\|\mathbf{a}(\boldsymbol{\eta})\|^2}. \tag{40}$$

Placing focus to the matrix element corresponding to $\boldsymbol{\eta}$, when the block inversion operation is again applied to $\mathbf{F}_{\boldsymbol{\eta}|\boldsymbol{\epsilon}}$, it yields

$$\mathbf{CRB}_{\boldsymbol{\eta}|\boldsymbol{\epsilon}} = \frac{\sigma_n^2}{2\alpha^2}\left[\boldsymbol{\Phi}_{\boldsymbol{\eta}|\boldsymbol{\epsilon}} - \frac{\mathrm{Im}\left\{\mathbf{a}(\boldsymbol{\eta})^H \frac{\partial \mathbf{a}(\boldsymbol{\eta})}{\partial \boldsymbol{\eta}^T}\right\}^T \mathrm{Im}\left\{\mathbf{a}(\boldsymbol{\eta})^H \frac{\partial \mathbf{a}(\boldsymbol{\eta})}{\partial \boldsymbol{\eta}^T}\right\}}{\|\mathbf{a}(\boldsymbol{\eta})\|^2 + \frac{\sigma_n^2}{2\alpha^2\sigma_{n_a}^2}}\right]^{-1}. \tag{41}$$

For the true parameter vector $\boldsymbol{\eta}^0$, the output signal-to-noise ratio (SNR) of the receiver matched filter is defined as [11]

$$\mathrm{SNR}_{\mathrm{out}} = \left. \frac{\mathrm{Re}\left\{ \left(\frac{\mathbf{a}(\eta)}{\|\mathbf{a}(\eta)\|} \right)^H \left(\alpha^0 \mathbf{a}\left(\eta^0\right) \right) \right\}^2}{\mathrm{E}\left[\mathrm{Re}\left\{ \left(\frac{\mathbf{a}(\eta)}{\|\mathbf{a}(\eta)\|} \right)^H \mathbf{n} \right\}^2 \right]} \right|_{\eta^0} = \frac{\left(\alpha^0\right)^2 \left\|\mathbf{a}\left(\eta^0\right)\right\|^2}{\frac{\left(\sigma_n^0\right)^2}{2}} = \frac{2\|\mathbf{a}\|^2}{\left(\sigma_n^0\right)^2} \left(\alpha^0\right)^2. \tag{42}$$

Using (42), the denominator in (41) can be rewritten as

$$\frac{1}{\|\mathbf{a}(\boldsymbol{\eta})\|^2 + \frac{\sigma_n^2}{2\alpha^2} \frac{1}{\sigma_{n_a}^2}} = \frac{1}{\|\mathbf{a}(\boldsymbol{\eta})\|^2 + \frac{\|\mathbf{a}(\boldsymbol{\eta})\|^2}{2\mathrm{SNR}_{\mathrm{out}} \sigma_{n_a}^2}} = \frac{1}{\|\mathbf{a}(\boldsymbol{\eta})\|^2 \left(1 + \frac{1}{2\mathrm{SNR}_{\mathrm{out}} \sigma_{n_a}^2}\right)}, \tag{43a}$$

$$= \frac{1}{\|\mathbf{a}(\boldsymbol{\eta})\|^2 \left(\frac{1+2\mathrm{SNR}_{\mathrm{out}} \sigma_{n_a}^2}{2\mathrm{SNR}_{\mathrm{out}} \sigma_{n_a}^2}\right)} = \frac{2\mathrm{SNR}_{\mathrm{out}} \sigma_{n_a}^2}{\|\mathbf{a}(\boldsymbol{\eta})\|^2 \left(1 + 2\mathrm{SNR}_{\mathrm{out}} \sigma_{n_a}^2\right)}, \tag{43b}$$

$$= \frac{1}{\|\mathbf{a}(\boldsymbol{\eta})\|^2} - \frac{1}{\|\mathbf{a}(\boldsymbol{\eta})\|^2 \left(1 + 2\sigma_{n_a}^2 \mathrm{SNR}_{\mathrm{out}}\right)}. \tag{43c}$$

Such result can be leveraged to refactor the righ-hand-side term in (41) as,

$$\frac{\mathrm{Im}\left\{ \mathbf{a}(\boldsymbol{\eta})^H \frac{\partial \mathbf{a}(\boldsymbol{\eta})}{\partial \eta^T} \right\}^T \mathrm{Im}\left\{ \mathbf{a}(\boldsymbol{\eta})^H \frac{\partial \mathbf{a}(\boldsymbol{\eta})}{\partial \eta^T} \right\}}{\|\mathbf{a}(\boldsymbol{\eta})\|^2 + \frac{\sigma_n^2}{2\alpha^2} \frac{1}{\sigma_{n_a}^2}}$$

$$= \frac{\mathrm{Im}\left\{ \mathbf{a}(\boldsymbol{\eta})^H \frac{\partial \mathbf{a}(\boldsymbol{\eta})}{\partial \eta^T} \right\}^T \mathrm{Im}\left\{ \mathbf{a}(\boldsymbol{\eta})^H \frac{\partial \mathbf{a}(\boldsymbol{\eta})}{\partial \eta^T} \right\}}{\|\mathbf{a}(\boldsymbol{\eta})\|^2} - \frac{\mathrm{Im}\left\{ \mathbf{a}(\boldsymbol{\eta})^H \frac{\partial \mathbf{a}(\boldsymbol{\eta})}{\partial \eta^T} \right\}^T \mathrm{Im}\left\{ \mathbf{a}(\boldsymbol{\eta})^H \frac{\partial \mathbf{a}(\boldsymbol{\eta})}{\partial \eta^T} \right\}}{\|\mathbf{a}(\boldsymbol{\eta})\|^2 \left(1 + 2\sigma_{n_a}^2 \mathrm{SNR}_{\mathrm{out}}\right)}, \tag{44}$$

which transforms (41) into,

$$\mathbf{CRB}_{\boldsymbol{\eta}|\boldsymbol{\epsilon}} = \frac{\sigma_n^2}{2\alpha^2} \left[\boldsymbol{\Phi}_{\boldsymbol{\eta}|\boldsymbol{\epsilon}} - \frac{\mathrm{Im}\left\{ \mathbf{a}(\boldsymbol{\eta})^H \frac{\partial \mathbf{a}(\boldsymbol{\eta})}{\partial \eta^T} \right\}^T \mathrm{Im}\left\{ \mathbf{a}(\boldsymbol{\eta})^H \frac{\partial \mathbf{a}(\boldsymbol{\eta})}{\partial \eta^T} \right\}}{\|\mathbf{a}(\boldsymbol{\eta})\|^2} + \frac{\mathrm{Im}\left\{ \mathbf{a}(\boldsymbol{\eta})^H \frac{\partial \mathbf{a}(\boldsymbol{\eta})}{\partial \eta^T} \right\}^T \mathrm{Im}\left\{ \mathbf{a}(\boldsymbol{\eta})^H \frac{\partial \mathbf{a}(\boldsymbol{\eta})}{\partial \eta^T} \right\}}{\|\mathbf{a}(\boldsymbol{\eta})\|^2 \left(1 + 2\sigma_{n_a}^2 \mathrm{SNR}_{\mathrm{out}}\right)} \right]^{-1}. \tag{45}$$

Additionally, the expression can be rewritten as

$$\mathbf{CRB}_{\boldsymbol{\eta}|\boldsymbol{\epsilon}} = \frac{\sigma_n^2}{2\alpha^2} \left(\boldsymbol{\Phi}_{\mathrm{CSM}}(\boldsymbol{\eta}) + \frac{\mathrm{Im}\left\{ \mathbf{a}(\boldsymbol{\eta})^H \frac{\partial \mathbf{a}(\boldsymbol{\eta})}{\partial \eta^T} \right\}^T \mathrm{Im}\left\{ \mathbf{a}(\boldsymbol{\eta})^H \frac{\partial \mathbf{a}(\boldsymbol{\eta})}{\partial \eta^T} \right\}}{\|\mathbf{a}(\boldsymbol{\eta})\|^2 \left(1 + 2\sigma_{n_a}^2 \mathrm{SNR}_{\mathrm{out}}\right)} \right)^{-1}, \tag{46}$$

where

$$\boldsymbol{\Phi}_{\mathrm{CSM}}(\boldsymbol{\eta}) = \mathrm{Re}\left\{ \left(\frac{\partial \mathbf{a}(\boldsymbol{\eta})}{\partial \boldsymbol{\eta}^T} \right)^H \Pi^{\perp}_{\mathbf{a}(\boldsymbol{\eta})} \frac{\partial \mathbf{a}(\boldsymbol{\eta})}{\partial \boldsymbol{\eta}^T} \right\}, \tag{47}$$

and

$$\boldsymbol{F}_{\mathrm{CSM}}(\boldsymbol{\eta}) = \frac{2\alpha^2}{\sigma_n^2} \boldsymbol{\Phi}_{\mathrm{CSM}}(\boldsymbol{\eta}), \tag{48}$$

denotes the conventional CSM FIM, as derived in previous studies [6, 19], where hardware and propagation-related terms are merged into a single complex amplitude parameter (1). Applying block matrix inversion to (39) finally yields the individual bounds,

$$CRB_{\varphi|\boldsymbol{\epsilon}} = \frac{\sigma_n^2}{2\alpha^2}\left[\frac{1}{\sigma_{n_a}^2} + \frac{1}{\frac{1}{2\mathrm{SNR}_{\mathrm{out}}} + \frac{\mathrm{Im}\left\{\mathbf{a}(\boldsymbol{\eta})^H \frac{\partial \mathbf{a}(\boldsymbol{\eta})}{\partial \boldsymbol{\eta}^T}\right\}^T \boldsymbol{F}_{\mathrm{CSM}}^{-1}(\boldsymbol{\eta}) \mathrm{Im}\left\{\mathbf{a}(\boldsymbol{\eta})^H \frac{\partial \mathbf{a}(\boldsymbol{\eta})}{\partial \boldsymbol{\eta}^T}\right\}}{\|\mathbf{a}(\boldsymbol{\eta})\|^4}}\right]^{-1}, \tag{49}$$

$$\mathbf{CRB}_{\boldsymbol{\eta},\varphi|\boldsymbol{\epsilon}} = -\mathbf{CRB}_{\boldsymbol{\eta}|\boldsymbol{\epsilon}} \frac{\mathrm{Im}\left\{\mathbf{a}(\boldsymbol{\eta})^H \frac{\partial \mathbf{a}(\boldsymbol{\eta})}{\partial \boldsymbol{\eta}^T}\right\}^T}{\|\mathbf{a}(\boldsymbol{\eta})\|^2} \frac{1}{1 + \frac{1}{2\mathrm{SNR}_{\mathrm{out}}\sigma_{n_a}^2}}. \tag{50}$$

It is worth noting that

$$CRB_{\varphi|\boldsymbol{\epsilon}} \geq \sigma_{n_a}^2 \frac{1}{1 + 2\sigma_{n_a}^2 \mathrm{SNR}_{\mathrm{out}}} = \frac{1}{2\mathrm{SNR}_{\mathrm{out}}} \frac{1}{1 + \frac{1}{2\sigma_{n_a}^2 \mathrm{SNR}_{\mathrm{out}}}}, \tag{51}$$

with equality if $\mathrm{Im}\left\{\mathbf{a}\,(\boldsymbol{\eta})^H \left(\frac{\partial \mathbf{a}(\boldsymbol{\eta})}{\partial \boldsymbol{\eta}^T}\right)\right\} = \mathbf{0}$.

5.1. Impact of auxiliary phase observables

This section applies the CRB expressions derived for the signal model incorporating auxiliary phase observables in equation (6), to the general TDE framework for signal transmission, where the parameter vector $\boldsymbol{\eta} = [\tau, \boldsymbol{\omega}]^T$ contains the time-delay τ variable as the primary parameter and/or additional unknown deterministic parameters (Doppler, DOA) modeled by $\boldsymbol{\omega}$. On the one side, the MLE derived in Section 4 applies directly to this general model without modification, as the MLE framework accommodates arbitrary parameterizations of $\boldsymbol{\eta}$. One the other side, the CRB for $\boldsymbol{\eta}$ in equation (46) reduces to

$$\mathbf{CRB}_{\boldsymbol{\eta}|\boldsymbol{\epsilon}} = \frac{\sigma_n^2}{2\alpha^2}\left[\mathrm{Re}\left\{\left(\frac{\partial \mathbf{c}(\boldsymbol{\eta})}{\partial \boldsymbol{\eta}^{\mathrm{T}}}\right)^H \Pi_{\mathbf{c}(\boldsymbol{\eta})}^{\perp} \frac{\partial \mathbf{c}(\boldsymbol{\eta})}{\partial \boldsymbol{\eta}^{\mathrm{T}}}\right\} + \boldsymbol{\Phi}(\boldsymbol{\eta})\right]^{-1}, \tag{52}$$

with,

$$\boldsymbol{\Phi}(\boldsymbol{\eta}) = \frac{\|\mathbf{c}(\boldsymbol{\eta})\|^2}{1 + 2\sigma_{n_a}^2 \mathrm{SNR}_{\mathrm{out}}}\left(2\pi f_c \mathbf{e}_1 - \frac{\mathrm{Im}\{\mathbf{c}(\boldsymbol{\eta})^H \frac{\partial \mathbf{c}(\boldsymbol{\eta})}{\partial \boldsymbol{\eta}^T}\}^T}{\|\mathbf{c}(\boldsymbol{\eta})\|^2}\right)\left(2\pi f_c \mathbf{e}_1 - \frac{\mathrm{Im}\{\mathbf{c}(\boldsymbol{\eta})^H \frac{\partial \mathbf{c}(\boldsymbol{\eta})}{\partial \boldsymbol{\eta}^T}\}^T}{\|\mathbf{c}(\boldsymbol{\eta})\|^2}\right)^T, \tag{53}$$

where $\mathbf{e}_1 = [1, \mathbf{0}^T]^T$ selects the time-delay parameter within $\boldsymbol{\eta}$. Consistent with the signal model specialization, the $\mathbf{CRB}_{\varphi|\boldsymbol{\epsilon}}$ accounting for the hardware-induced phase

offset φ modifies to

$$CRB_{\varphi|\boldsymbol{\epsilon}} = \left(\frac{1}{\sigma_{n_a}^2} + \frac{1}{\frac{1}{2\mathrm{SNR}_{\mathrm{out}}} + \left(2\pi f_c \mathbf{e}_1 - \frac{\mathrm{Im}\{\mathbf{c}(\boldsymbol{\eta})^H \frac{\partial \mathbf{c}(\boldsymbol{\eta})}{\partial \boldsymbol{\eta}^T}\}}{\|\mathbf{c}(\boldsymbol{\eta})\|^2} \right)^T \mathbf{CRB}_{\boldsymbol{\eta}|\boldsymbol{\epsilon}} \left(2\pi f_c \mathbf{e}_1 - \frac{\mathrm{Im}\{\mathbf{c}(\boldsymbol{\eta})^H \frac{\partial \mathbf{c}(\boldsymbol{\eta})}{\partial \boldsymbol{\eta}^T}\}}{\|\mathbf{c}(\boldsymbol{\eta})\|^2} \right)} \right)^{-1}. \tag{54}$$

Following the same signal model specialization, the cross-information terms adapt to

$$\mathbf{CRB}_{\boldsymbol{\eta},\varphi|\boldsymbol{\epsilon}} = \mathbf{CRB}_{\boldsymbol{\eta}|\boldsymbol{\epsilon}} \left(2\pi f_c \mathbf{e}_1 - \frac{\mathrm{Im}\{\mathbf{c}(\boldsymbol{\eta})^H \frac{\partial \mathbf{c}(\boldsymbol{\eta})}{\partial \boldsymbol{\eta}^T}\}}{\|\mathbf{c}(\boldsymbol{\eta})\|^2} \right)^T \frac{1}{1 + \frac{1}{2\mathrm{SNR}_{\mathrm{out}} \sigma_{n_a}^2}}. \tag{55}$$

5.2. Analysis of global phase estimation

The global phase $\phi = \varphi - 2\pi f_c \tau$ merges hardware-induced and propagation-induced phase components. That formulation corresponds to rearranging the signal model in equation (3) by explicitly extracting the time-delay dependent carrier-phase term $e^{-j2\pi f_c \tau}$ from $\psi(\boldsymbol{\eta})$ and merging it with the hardware phase φ, while maintaining τ as a separate parameter within $\boldsymbol{\eta}$. The CRB for the global phase derives from the linear transformation

$$\phi = \varphi - 2\pi f_c \tau = \begin{bmatrix} 1 \\ \boldsymbol{\lambda} \end{bmatrix}^T \boldsymbol{\theta}, \quad \boldsymbol{\lambda} = \begin{bmatrix} -2\pi f_c \\ \mathbf{0} \end{bmatrix} = -2\pi f_c \mathbf{e}_1, \quad \mathbf{e}_1 = \begin{bmatrix} 1 \\ \mathbf{0} \end{bmatrix}. \tag{56}$$

Application of the covariance transformation formula [11] yields

$$CRB_{\phi|\boldsymbol{\epsilon}} = \begin{bmatrix} 1 \\ \boldsymbol{\lambda} \end{bmatrix}^T \mathbf{CRB}_{\boldsymbol{\theta}|\boldsymbol{\epsilon}} \begin{bmatrix} 1 \\ \boldsymbol{\lambda} \end{bmatrix}. \tag{57}$$

Under the limiting case $\sigma_{n_a}^2 \to \infty$, i.e. no additional phase information, firstly

$$\mathbf{CRB}_{\boldsymbol{\eta}|\boldsymbol{\epsilon}} = \frac{\sigma_n^2}{2\alpha^2} \mathrm{Re} \left\{ \left(\frac{\partial \mathbf{c}(\boldsymbol{\eta})}{\partial \boldsymbol{\eta}^{\mathrm{T}}} \right)^H \Pi_{\mathbf{c}(\boldsymbol{\eta})}^{\perp} \frac{\partial \mathbf{c}(\boldsymbol{\eta})}{\partial \boldsymbol{\eta}^{\mathrm{T}}} \right\}^{-1}, \tag{58}$$

coincides with the conventional CSM CRB. Secondly, substituting the cross-term from equation (50) leads to

$$CRB_{\phi|\boldsymbol{\epsilon}} = CRB_{\varphi|\boldsymbol{\epsilon}} - \frac{4\pi f_c}{\|\mathbf{a}(\boldsymbol{\eta})\|^2} \mathbf{e}_1^T \mathrm{Im} \left\{ \mathbf{a}(\boldsymbol{\eta})^H \frac{\partial \mathbf{a}(\boldsymbol{\eta})}{\partial \boldsymbol{\eta}^T} \right\}^T \mathbf{CRB}_{\boldsymbol{\eta}|\boldsymbol{\epsilon}} + (2\pi f_c)^2 \mathbf{e}_1^T \mathbf{CRB}_{\boldsymbol{\eta}|\boldsymbol{\epsilon}} \mathbf{e}_1. \tag{59}$$

The derivative relationships for the time-delay signal model are

$$\frac{\partial \mathbf{a}(\boldsymbol{\eta})}{\partial \boldsymbol{\eta}^T} = \left(-\mathbf{c}(\boldsymbol{\eta}) j 2\pi f_c \mathbf{e}_1 + \frac{\partial \mathbf{c}(\boldsymbol{\eta})}{\partial \boldsymbol{\eta}^T} \right) e^{-j2\pi f_c \tau}, \tag{60a}$$

$$\mathbf{a}(\boldsymbol{\eta})^H \frac{\partial \mathbf{a}(\boldsymbol{\eta})}{\partial \boldsymbol{\eta}^T} = -\|\mathbf{c}(\boldsymbol{\eta})\|^2 j 2\pi f_c \mathbf{e}_1^T + \mathbf{c}(\boldsymbol{\eta})^H \frac{\partial \mathbf{c}(\boldsymbol{\eta})}{\partial \boldsymbol{\eta}^T}. \tag{60b}$$

Using $\|\mathbf{a}(\boldsymbol{\eta})\|^2 \equiv \|\mathbf{c}(\boldsymbol{\eta})\|^2$, equation (59) becomes,

$$CRB_{\phi|\boldsymbol{\epsilon}} = CRB_{\varphi|\boldsymbol{\epsilon}} + \frac{4\pi f_c}{\|\mathbf{c}(\boldsymbol{\eta})\|^2}\mathbf{e}_1^T \mathrm{Im}\left\{\mathbf{c}(\boldsymbol{\eta})^H \frac{\partial \mathbf{c}(\boldsymbol{\eta})}{\partial \boldsymbol{\eta}^T}\right\}^T \mathbf{CRB}_{\boldsymbol{\eta}|\boldsymbol{\epsilon}} - (2\pi f_c)^2 \mathbf{e}_1^T \mathbf{CRB}_{\boldsymbol{\eta}|\boldsymbol{\epsilon}} \mathbf{e}_1. \quad (61)$$

Expressing $CRB_{\varphi|\boldsymbol{\epsilon}}$ from equation (49) using equation (60)

$$\begin{aligned} CRB_{\varphi|\boldsymbol{\epsilon}} = \frac{1}{2\mathrm{SNR}_{\mathrm{out}}} + \frac{1}{\|\mathbf{c}(\boldsymbol{\eta})\|^4} \mathrm{Im}\left\{\mathbf{c}(\boldsymbol{\eta})^H \frac{\partial \mathbf{c}(\boldsymbol{\eta})}{\partial \boldsymbol{\eta}^T}\right\} \mathbf{CRB}_{\boldsymbol{\eta}|\boldsymbol{\epsilon}} \mathrm{Im}\left\{\mathbf{c}(\boldsymbol{\eta})^H \frac{\partial \mathbf{c}(\boldsymbol{\eta})}{\partial \boldsymbol{\eta}^T}\right\}^T \\ - \frac{4\pi f_c}{\|\mathbf{c}(\boldsymbol{\eta})\|^2} \mathrm{Im}\left\{\mathbf{c}(\boldsymbol{\eta})^H \frac{\partial \mathbf{c}(\boldsymbol{\eta})}{\partial \boldsymbol{\eta}^T}\right\} \mathbf{CRB}_{\boldsymbol{\eta}|\boldsymbol{\epsilon}} \mathbf{e}_1 + (2\pi f_c)^2 \mathbf{e}_1^T \mathbf{CRB}_{\boldsymbol{\eta}|\boldsymbol{\epsilon}} \mathbf{e}_1. \quad (62) \end{aligned}$$

Substituting equation (62) into equation (61) produces systematic cancellation of carrier frequency-dependent terms, yielding

$$CRB_{\phi|\boldsymbol{\epsilon}} = \frac{1}{2\mathrm{SNR}_{\mathrm{out}}} + \frac{1}{\|\mathbf{c}(\boldsymbol{\eta})\|^4} \mathrm{Im}\left\{\mathbf{c}(\boldsymbol{\eta})^H \frac{\partial \mathbf{c}(\boldsymbol{\eta})}{\partial \boldsymbol{\eta}^T}\right\} \mathbf{CRB}_{\boldsymbol{\eta}|\boldsymbol{\epsilon}} \mathrm{Im}\left\{\mathbf{c}(\boldsymbol{\eta})^H \frac{\partial \mathbf{c}(\boldsymbol{\eta})}{\partial \boldsymbol{\eta}^T}\right\}^T. \quad (63)$$

By comparing $CRB_{\phi|\boldsymbol{\epsilon}}$ (63) against $CRB_{\varphi|\boldsymbol{\epsilon}}$ in equation (62), one observes that $CRB_{\phi|\boldsymbol{\epsilon}}$ lacks the $(2\pi f_c)^2$ and $(4\pi f_c)$ amplification terms affecting $CRB_{\varphi|\boldsymbol{\epsilon}}$ (62). Hence, it is expected to provide a smaller variance (always true for real-valued baseband signals), providing theoretical justification for conventional approaches that estimate merged phase parameters, when no additional hardware-induced phase measurements are available.

6. Asymptotic covariance

The purpose of this section is to derive an approximate expression for the covariance matrix of the MLE associated with the observation model in (6), as introduced in Section 4, and to demonstrate that its converges to the corresponding Cramér–Rao bound in the high-SNR regime. This analysis is motivated by the asymptotic performance plateau observed in previous empirical covariance estimation based on a Taylor-series expansion, which suggested an apparent limitation due to the phase-noise variance $\sigma_{n_a}^2$ (see [20] and Section 7.2). The derivation obtained with the well-known Fisher Scoring Method [21, 22, 23, 24] reveals that this limitation is only an artifact of the previous analysis and that the MLE is asymptotically efficient. For readability and brevity, only the main steps of the derivation are presented; the complete proof is provided in the Technical Note [25].

6.1. MLE cost function

The MLE is obtained by minimizing the conditional negative log-likelihood function in (18)

$$F(\boldsymbol{\theta}; \boldsymbol{\theta}^0) = \left\| \Pi^{\perp}_{\underline{\mathbf{a}}(\boldsymbol{\eta})} \underline{\mathbf{x}} \right\|^2 + \frac{(x_a - \varphi)^2}{2\sigma_{n_a}^2}, \quad (64)$$

where

$$\underline{\mathbf{x}}(\boldsymbol{\zeta}^0) = \underline{\mathbf{b}}(\boldsymbol{\theta}^0)\alpha^0 + \underline{\mathbf{n}}, \quad (65)$$

with

$$\underline{\mathbf{n}} \sim \mathcal{N}\left(\mathbf{0}, \frac{\sigma_n^2}{2}\mathbf{I}_{2N}\right). \quad (66)$$

The parameter vector is defined as $\boldsymbol{\theta}^T = (\varphi, \boldsymbol{\eta}^T)$ with $\boldsymbol{\eta} \in \mathbb{R}^K$. Using the projector properties $\Pi^{\perp}_{\underline{\mathbf{b}}} = \mathbf{I} - \Pi_{\underline{\mathbf{b}}}$, and $\Pi_{\underline{\mathbf{b}}} = \underline{\mathbf{b}} \left(\underline{\mathbf{b}}^T \underline{\mathbf{b}}\right)^{-1} \underline{\mathbf{b}}^T$, the cost function can be rewritten as

$$F(\boldsymbol{\theta}; \boldsymbol{\theta}^0) = \mathrm{tr}\left(\Pi^{\perp}_{\underline{\mathbf{b}}(\boldsymbol{\theta})} \, \underline{\mathbf{x}}(\boldsymbol{\zeta}^0) \underline{\mathbf{x}}^T(\boldsymbol{\zeta}^0)\right) + \frac{\sigma_n^2}{2\sigma_{n_a}^2} \left(x_a(\varphi^0) - \mathbf{e}_1{}^T \boldsymbol{\theta}\right)^2, \tag{67}$$

where $\mathbf{e}_1 = [1, 0, \ldots, 0]^T \in \mathbb{R}^{K+1}$ denotes the first canonical basis vector, so that $\mathbf{e}_1^T \boldsymbol{\theta} = \varphi$.

6.2. Linearization of the estimator

Since $\hat{\boldsymbol{\theta}}$ is an extremum of $F(\boldsymbol{\theta}; \boldsymbol{\theta}^0)$,

$$\mathbf{0} = \left.\frac{\partial F(\boldsymbol{\theta}; \boldsymbol{\theta}^0)}{\partial \boldsymbol{\theta}}\right|_{\hat{\boldsymbol{\theta}}}. \tag{68}$$

If $\hat{\boldsymbol{\theta}}$ is close to $\boldsymbol{\theta}^0$, a first-order Taylor expansion yields

$$\mathbf{0} \simeq \left.\frac{\partial F(\boldsymbol{\theta}; \boldsymbol{\theta}^0)}{\partial \boldsymbol{\theta}}\right|_{\boldsymbol{\theta}^0} + \left.\frac{\partial^2 F(\boldsymbol{\theta}; \boldsymbol{\theta}^0)}{\partial \boldsymbol{\theta} \partial \boldsymbol{\theta}^T}\right|_{\boldsymbol{\theta}^0} (\hat{\boldsymbol{\theta}} - \boldsymbol{\theta}^0). \tag{69}$$

Hence,

$$\hat{\boldsymbol{\theta}} \simeq \boldsymbol{\theta}^0 - \mathbf{J}^{-1}\mathbf{g}, \quad \text{with} \quad \mathbf{J} = \left.\frac{\partial^2 F(\boldsymbol{\theta}; \boldsymbol{\theta}^0)}{\partial \boldsymbol{\theta} \partial \boldsymbol{\theta}^T}\right|_{\boldsymbol{\theta}^0}, \quad \mathbf{g} = \left.\frac{\partial F(\boldsymbol{\theta}; \boldsymbol{\theta}^0)}{\partial \boldsymbol{\theta}}\right|_{\boldsymbol{\theta}^0}. \tag{70}$$

6.3. Fisher scoring approximation

In practice, the observed Hessian $\mathbf{J}$ is often replaced by its expectation under the true parameters, leading to the Fisher scoring iteration,

$$\hat{\boldsymbol{\theta}} \simeq \boldsymbol{\theta}^0 - \mathbf{J}_E^{-1}\mathbf{g}, \quad \text{where} \quad \mathbf{J}_E = E_{\boldsymbol{\zeta}^0}\left[\left.\frac{\partial^2 F(\boldsymbol{\theta}; \boldsymbol{\theta}^0)}{\partial \boldsymbol{\theta} \partial \boldsymbol{\theta}^T}\right|_{\boldsymbol{\theta}^0}\right]. \tag{71}$$

That approximation improves numerical stability and facilitates the analytical computation of the asymptotic estimator covariance [21, 22, 23, 24].

6.4. General covariance expression

Taking expectations of $(\hat{\boldsymbol{\theta}} - \boldsymbol{\theta}^0)(\hat{\boldsymbol{\theta}} - \boldsymbol{\theta}^0)^T$ gives the general form:

$$\mathbf{C}_{\hat{\boldsymbol{\theta}}} = E_{\boldsymbol{\zeta}^0}\left[(\hat{\boldsymbol{\theta}} - \boldsymbol{\theta}^0)(\hat{\boldsymbol{\theta}} - \boldsymbol{\theta}^0)^T\right] \simeq \mathbf{J}_E^{-1} \mathbf{H}_E \mathbf{J}_E^{-1}, \tag{72}$$

where

$$\mathbf{J}_E = E_{\boldsymbol{\zeta}^0}\left[\left.\frac{\partial^2 F}{\partial \boldsymbol{\theta} \partial \boldsymbol{\theta}^T}\right|_{\boldsymbol{\theta}^0}\right], \qquad \mathbf{H}_E = E_{\boldsymbol{\zeta}^0}\left[\left.\frac{\partial F}{\partial \boldsymbol{\theta}} \frac{\partial F}{\partial \boldsymbol{\theta}^T}\right|_{\boldsymbol{\theta}^0}\right]. \tag{73}$$

6.5. Expected gradient and hessian computation

Starting from the structure of $F(\boldsymbol{\theta}; \boldsymbol{\theta}^0)$, the partial derivatives are

$$\frac{\partial F}{\partial \boldsymbol{\theta}} = \frac{\partial}{\partial \boldsymbol{\theta}} \mathrm{tr}\left(\Pi^{\perp}_{\mathbf{b}(\boldsymbol{\theta})} \mathbf{x}\mathbf{x}^T\right) + \frac{\sigma_n^2}{\sigma_{n_a}^2} (\varphi - x_a(\varphi^0)) \mathbf{e}_1, \tag{74}$$

$$\frac{\partial^2 F}{\partial \boldsymbol{\theta} \partial \boldsymbol{\theta}^T} = \frac{\partial^2}{\partial \boldsymbol{\theta} \partial \boldsymbol{\theta}^T} \mathrm{tr}\left(\Pi^{\perp}_{\mathbf{b}(\boldsymbol{\theta})} \mathbf{x}\mathbf{x}^T\right) + \frac{\sigma_n^2}{\sigma_{n_a}^2} \mathbf{e}_1 \mathbf{e}_1{}^T, \tag{75}$$

by using projector identities such as $\Pi_{\mathbf{b}}^{\perp}\mathbf{b} = \mathbf{0}$ and $\frac{\partial \Pi_{\mathbf{b}}^{\perp}}{\partial \theta_k}\mathbf{b} = -\Pi_{\mathbf{b}}^{\perp}\frac{\partial \mathbf{b}}{\partial \theta_k}$, the expected Hessian can be shown to be [25]

$$E_{\zeta^0}\left[\frac{\partial^2 F}{\partial \boldsymbol{\theta}\partial \boldsymbol{\theta}^T}\right]_{\boldsymbol{\theta}^0} = \sigma_n^2\,\mathbf{CRB}_{\boldsymbol{\theta}|\boldsymbol{\zeta}}^{-1}(\boldsymbol{\zeta}^0), \tag{76}$$

which connects directly to the Fisher information structure of the conditional model. Similarly, the expected outer product of the gradient gives [25]

$$E_{\zeta^0}\left[\frac{\partial F}{\partial \boldsymbol{\theta}}\frac{\partial F}{\partial \boldsymbol{\theta}^T}\right]_{\boldsymbol{\theta}^0} = (\sigma_n^2)^2\left(\mathbf{CRB}_{\boldsymbol{\theta}|\boldsymbol{\zeta}}^{-1}(\boldsymbol{\zeta}^0) + \frac{\boldsymbol{\Phi}^{CSM}(\boldsymbol{\theta}^0)}{\|\mathbf{a}(\boldsymbol{\eta}^0)\|^2}\right), \tag{77}$$

where $\boldsymbol{\Phi}^{CSM}(\boldsymbol{\theta})$ denotes the *conditional statistical model* information matrix

$$\boldsymbol{\Phi}^{CSM}(\boldsymbol{\theta}) = \frac{\partial \mathbf{b}(\boldsymbol{\theta})^T}{\partial \boldsymbol{\theta}}\Pi_{\mathbf{b}(\boldsymbol{\theta})}^{\perp}\frac{\partial \mathbf{b}(\boldsymbol{\theta})}{\partial \boldsymbol{\theta}^T}. \tag{78}$$

6.6. Asymptotic covariance expression

By substituting (76) and (77) into (72), the asymptotic covariance of the where CMLE denotes the *Conditional MLE* can be expressed as

$$\mathbf{C}_{\hat{\boldsymbol{\theta}}} \simeq \mathbf{CRB}_{\boldsymbol{\theta}|\boldsymbol{\zeta}}(\boldsymbol{\zeta}^0) + \mathbf{CRB}_{\boldsymbol{\theta}|\boldsymbol{\zeta}}(\boldsymbol{\zeta}^0)\left(\frac{\boldsymbol{\Phi}^{CSM}(\boldsymbol{\theta}^0)}{\|\mathbf{a}(\boldsymbol{\eta}^0)\|^2}\right)\mathbf{CRB}_{\boldsymbol{\theta}|\boldsymbol{\zeta}}(\boldsymbol{\zeta}^0). \tag{79}$$

Equation (79) reveals that the asymptotic covariance matrix consists of two components:

- the **conditional CRB** term, representing the theoretical lower bound on the estimation variance under ideal model conditions;
- a **correction term**, proportional to the normalized CSM information matrix $\boldsymbol{\Phi}^{CSM}(\boldsymbol{\theta}^0)/\|\mathbf{a}(\boldsymbol{\eta}^0)\|^2$, accounting for residual coupling between parameters.

As either the signal-to-noise ratio or the number of samples increases, the correction term becomes negligible, and the MLE *asymptotically converges to the CRB*. That demonstrates that the estimator achieves full efficiency at high SNR, contrary to the apparent performance saturation that might be expected due to the phase noise variance $\sigma_{n_a}^2$. It should be noted that (79) differs from Eq. (4.73) in [26] because it is derived from the score function defined in (64), which follows a different parameterization of the likelihood function [25].

7. Time-delay and Doppler estimation analysis

Considering the signal model in (6) and the narrowband assumption, the derivatives of the received signal with respect to the parameter vector $\boldsymbol{\eta}$ are given in continuous time by

$$\frac{\partial a(t;\boldsymbol{\eta})}{\partial \boldsymbol{\eta}} = \begin{pmatrix} \frac{\partial a(t;\boldsymbol{\eta})}{\partial \tau} \\ \frac{\partial a(t;\boldsymbol{\eta})}{\partial b} \end{pmatrix} = -\begin{pmatrix} \dot{c}(t-\tau) + jw_c(1-b)c(t-\tau) \\ jw_c(t-\tau)c(t-\tau) \end{pmatrix} e^{-j\psi(t;\boldsymbol{\eta})}, \tag{80}$$

where $\dot{c}(t-\tau)$ is the first time-derivative of $c(t-\tau)$. This expression can again be written in matrix form as,

$$\frac{\partial a(t;\boldsymbol{\eta})}{\partial \boldsymbol{\eta}} = -\mathbf{Q}\mathbf{v}(t-\tau)e^{-j\psi(t;\boldsymbol{\eta})}, \tag{81}$$

where

$$\mathbf{Q} = \begin{bmatrix} jw_c(1-b) & 0 & 1 \\ 0 & jw_c & 0 \end{bmatrix}, \quad \mathbf{v}'(t-\tau) = \begin{bmatrix} c(t-\tau) \\ (t-\tau)c(t-\tau) \\ \dot{c}(t-\tau) \end{bmatrix}. \tag{82}$$

The matrix $\mathbf{Q}$ can be directly compared with the corresponding matrix derived from the conventional CSM in [6, §11], showing that the presence of the factor $(1-b)$, instead of just b, is the key structural difference between the phase-compensated and conventional narrow-band formulations. These terms allow to express the FIM derivatives in equation (46) as,

$$\left(\frac{\partial a(t;\boldsymbol{\eta})}{\partial \boldsymbol{\eta}^{\mathrm{T}}}\right)^H \frac{\partial a(t;\boldsymbol{\eta})}{\partial \boldsymbol{\eta}^T} = \mathbf{Q}\Big(\mathbf{v}(t-\tau)\,\mathbf{v}^H(t-\tau)\Big)\mathbf{Q}^H, \tag{83a}$$

$$a(t;\boldsymbol{\eta})^H \frac{\partial a(t;\boldsymbol{\eta})}{\partial \boldsymbol{\eta}^T} = -\Big(\mathbf{v}(t-\tau)c^*(t;\boldsymbol{\eta})\Big)^T \mathbf{Q}^T, \tag{83b}$$

for which the Nyquist-Shannon theorem establishes the equivalence

$$\lim_{(N_1',N_2')\to(-\infty,\infty)} T_s \sum_{n=N_1'}^{N_2'} \mathbf{v}(nT_s;\boldsymbol{\eta})\,\mathbf{v}^H(nT_s;\boldsymbol{\eta}) = \int_{-\infty}^{\infty} \mathbf{v}(t;\boldsymbol{\eta})\,\mathbf{v}^H(t;\boldsymbol{\eta})\,dt = \mathbf{W}, \tag{84a}$$

$$\lim_{(N_1',N_2')\to(-\infty,\infty)} T_s \sum_{n=N_1'}^{N_2'} \mathbf{v}(nT_s;\boldsymbol{\eta})\,c^*(nT_s;\boldsymbol{\eta}) = \int_{-\infty}^{\infty} \mathbf{v}(t;\boldsymbol{\eta})\,c^*(t;\boldsymbol{\eta})\,dt = \mathbf{w}. \tag{84b}$$

where the vector $\mathbf{w}$ and matrix $\mathbf{W}$ contain the signal correlation terms

$$\mathbf{w} = \begin{pmatrix} w_1 \\ w_2 \\ w_3 \end{pmatrix}, \quad \mathbf{W} = \begin{bmatrix} w_1 & w_2^* & w_3^* \\ w_2 & W_{2,2} & w_4^* \\ w_3 & w_4 & W_{3,3} \end{bmatrix}, \tag{85}$$

whose individual elements are derived in [19, §A.2]. The result in (84) leads to the following reformulation of the derivatives in equation (83),

$$\left(\frac{\partial \mathbf{a}(\boldsymbol{\eta})}{\partial \boldsymbol{\eta}^T}\right)^H \frac{\partial \mathbf{a}(\boldsymbol{\eta})}{\partial \boldsymbol{\eta}^T} = f_s\mathbf{Q}\mathbf{W}\mathbf{Q}^H, \quad \mathbf{a}(\boldsymbol{\eta})^H \frac{\partial \mathbf{a}(\boldsymbol{\eta})}{\partial \boldsymbol{\eta}^T} = -f_s\,(\mathbf{Q}\mathbf{w})^T, \tag{86}$$

and consequently, the closed-form expression of the CRB in equation (46) reads,

$$\mathbf{CRB}_{\boldsymbol{\eta}|\boldsymbol{\epsilon}} = \frac{f_s w_1}{2\mathrm{SNR}_{\mathrm{out}}}\left(\mathrm{Re}\left\{\mathbf{Q}\mathbf{W}\mathbf{Q}^H\right\} - \frac{\mathrm{Re}\left\{(\mathbf{Q}\mathbf{w})^H(\mathbf{Q}\mathbf{w})\right\}^T}{w_1} + \frac{\mathrm{Im}\left\{(\mathbf{Q}\mathbf{w})^H(\mathbf{Q}\mathbf{w})\right\}^T}{w_1(1+2\sigma_{n_a}^2\mathrm{SNR}_{\mathrm{out}})}\right)^{-1}. \tag{87}$$

7.1. Delay-only scenario

This subsection considers a simplified scenario that assumes negligible Doppler effects, either due to short observation intervals or stationary propagation conditions, significantly reducing computational burden while preserving the essential structure for theoretical validation. That static scenario forms the basis for the numerical simulations presented in Section 10. Under that assumption, the parameter vector reduces to $\boldsymbol{\eta} = \tau$, and the optimization problem simplifies to

$$\widehat{\tau} = \arg\min_{\tau} \{\mathcal{S}_2(\mathbf{x}, x_a; \widehat{\varepsilon}(\tau), \tau)\} = \arg\min_{\tau} \left\{ \frac{\sigma_n^2 \widehat{\varepsilon}(\tau)^2}{2\sigma_{n_a}^2} - \mathrm{Re}\left\{ e^{-j\widehat{\varepsilon}(\tau)} \gamma(\tau) \right\}^2 \right\}. \tag{88}$$

Under the delay-only narrow-band assumption, the derivative terms from equation (80) reduce to

$$\frac{\partial a(t;\tau)}{\partial \tau} = -\begin{pmatrix} \dot{c}(t-\tau) + jw_c c(t-\tau) \end{pmatrix} e^{-jw_c\tau} = -\mathbf{Q}'\mathbf{v}'(t-\tau)e^{-jw_c\tau}. \tag{89}$$

with

$$\mathbf{Q}' = \begin{bmatrix} jw_c & 1 \end{bmatrix}, \quad \mathbf{v}'(t-\tau) = \begin{bmatrix} c(t-\tau) \\ \dot{c}(t-\tau) \end{bmatrix}, \quad \mathbf{W}' = \begin{bmatrix} w_1 & w_3^* \\ w_3 & W_{3,3} \end{bmatrix}, \quad \mathbf{w}' = \begin{bmatrix} w_1 \\ w_3 \end{bmatrix}. \tag{90a}$$

Consequently, (7) becomes,

$$\mathrm{CRB}_{\tau|\boldsymbol{\epsilon}} = \frac{f_s w_1}{2\mathrm{SNR}_{\mathrm{out}}} \left(\mathrm{Re}\left\{ \mathbf{Q}'\mathbf{W}'\mathbf{Q}'^H \right\} - \frac{\mathrm{Re}\left\{ (\mathbf{Q}'\mathbf{w}')^H (\mathbf{Q}'\mathbf{w}') \right\}^T}{w_1} + \frac{\mathrm{Im}\left\{ (\mathbf{Q}'\mathbf{w}')^H (\mathbf{Q}'\mathbf{w}') \right\}^T}{w_1 (1 + 2\sigma_{n_a}^2 \mathrm{SNR}_{\mathrm{out}})} \right)^{-1}. \tag{91}$$

7.2. Impact of Taylor-series approximation order

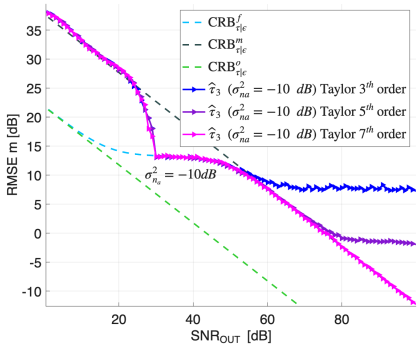
To evaluate the influence of the Taylor-series approximation order on the estimation performance, numerical simulations were carried out for both GPS L1 C/A and Kasami signals. Unless otherwise specified, the simulation setup remains unchanged throughout the paper and is summarized in Fig. 1a. The corresponding estimation results are reported in Fig. 1b. The derivation of the asymptotic covariance matrix provides insight into the origin of the second performance plateau observed in the numerical simulations. As illustrated in Fig. 1b, this plateau is not caused by the phase-noise variance $\sigma_{n_a}^2$, but rather by the truncation of the Taylor-series expansion used to approximate the nonlinear phase term in the CMLE cost function. The cyan curves correspond to the proposed conditional Cramér–Rao Bound in (45), whereas the gray curve represents the conventional CRB in (47), corresponding to the limiting case of infinite phase uncertainty. The green curve denotes the lower bound obtained under perfect phase knowledge. Finally, the blue, purple, and magenta curves represent the RMSE of the phase-aware estimator $\hat{\tau}_3$ in (88) obtained using third-, fifth-, and seventh-order Taylor-series approximations, respectively, for $\sigma_{n_a}^2 = -10$ dB. In particular, when the phase component is approximated using a third-order Taylor expansion, significant residual nonlinearities remain, leading to a pronounced performance plateau that limits the estimation accuracy even at high SNR [20]. Extending the approximation to the fifth order improves the representation of the phase term, although numerical instabilities may still affect the asymptotic behavior. Conversely, the seventh-order expansion substantially reduces the residual nonlinearities, improves numerical stability, and removes the approximation-induced plateau

over a broad range of $\sigma_{n_a}^2$ values for both GPS L1 C/A [1] and Kasami [27] signals. These results confirm that the observed saturation originates from the Taylor-series approximation rather than from an intrinsic limitation imposed by phase noise, in agreement with the asymptotic covariance analysis.

Simulation Setup and Taylor-Series Approximation

Parameter	GPS	Kasami
f_c	1575.42 MHz	225 kHz
f_0	1.023 MHz	15 kHz
f_s	4 MHz	30 kHz
Code length	1023	15
MC runs	1000	1000
τ_0	0	0
b_0	0, 10^{-8}	0, 10^{-8}
α	1	1
SNR_{out}	0–130 dB	0–130 dB
Delay grid	Uniform	Uniform
Doppler grid	$b_0 \pm 3\sigma_{\text{doppler}}$	
Bins	21	
$\sigma_{n_a}^2$	$\{-30, -20, -10\}$ dB	
Evaluated Bounds		
CRB^{m}	Merged phase	
CRB^{o}	Known phase	
CRB^{p}	Known phase + Doppler compensation	
CRB^{f}	Finite phase uncertainty	
RMSE m [dB]	$10\log_{10}\left(\frac{c}{f_0}\text{RMSE}\right)$	

(**a**) Simulation parameters.



(**b**) Taylor-series approximations of increasing order for the Kasami-coded waveform. Higher-order expansions provide a more accurate representation of the nonlinear phase term and reduce the approximation-induced performance plateau observed in the CMLE simulations.

Figure 1: Simulation setup and Taylor-series approximation. Panel (a) summarizes the simulation parameters and evaluated CRBs, while panel (b) illustrates the effect of the Taylor-series approximation order on estimation performance.

8. Ambiguity function analysis

The ambiguity function provides fundamental insight into the behavior of the maximum likelihood estimator and the role of carrier-phase information in time-delay estimation. Under the delay-only assumption described in Section 7.1, the received signal is an amplitude-scaled and time-delayed replica of the transmitted waveform, allowing the matched-filter response to be characterized through the ambiguity function. For ambiguity-function visualization purposes, the sampling and carrier frequencies are normalized with respect to the chip rate f_{chip}. Specifically, we define

$$F_s = \frac{f_s}{f_{\text{chip}}}, \qquad F_c = \frac{f_c}{f_{\text{chip}}}, \tag{92}$$

where f_s and f_c denote the physical sampling and carrier frequencies, respectively. The quantities F_s and F_c are therefore dimensionless parameters expressed in chip-rate units. These normalized parameters are used throughout this section to illustrate the

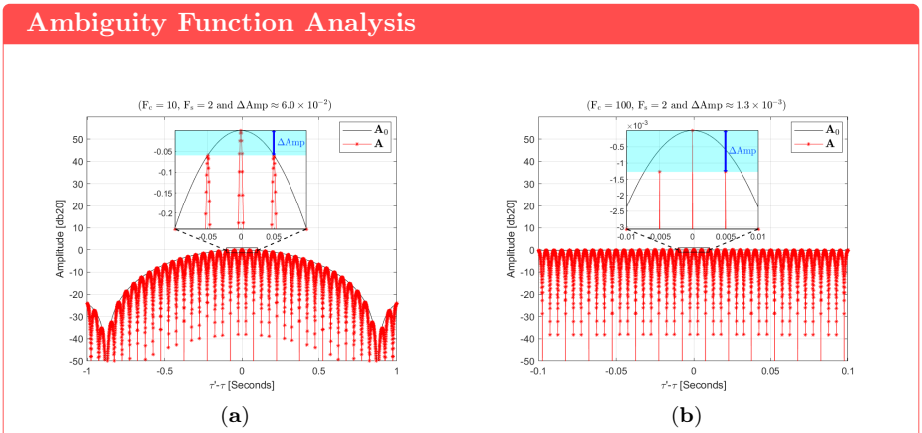


Figure 2: Ambiguity function of the GPS L1 C/A signal for different carrier frequencies. (a) $F_s = 2$, $F_c = 10$: ambiguity function with three visible lobes. (b) $F_s = 2$, $F_c = 100$: denser lobe pattern in the zoomed delay interval due to the higher carrier frequency. The lobe spacing is $\Delta\tau = 1/(2f_c)$, showing that increasing F_c improves timing resolution.

impact of sampling- and carrier-frequency scaling on the ambiguity-function structure shown in Fig. 2. Under high SNR conditions, i.e., $\sigma_n^2 \to 0$ and $\sigma_{na}^2 \to 0$, the discrete-time ambiguity function for the conditional signal model is given by

$$\Xi(\tau';\tau^0) = (\alpha^0)^2 \|\mathbf{a}(\tau^0)\|^2 \mathrm{Re}\left\{ \frac{\mathbf{a}(\tau')^H \mathbf{a}(\tau^0)}{\|\mathbf{a}(\tau')\| \, \|\mathbf{a}(\tau^0)\|} \right\}^2, \tag{93}$$

where $\tau' = \tau^0 + d\tau$ denotes a delay offset from the true delay τ^0. By exploiting the signal structure $\mathbf{a}(\tau) = \mathbf{c}(\tau)e^{j\psi(\tau)}$, with $\psi(\tau) = -\omega_c\tau$, we obtain

$$\Xi(\tau';\tau^0) = (\alpha^0)^2 \|\mathbf{c}(\tau^0)\|^2 \mathrm{Re}\left\{ \frac{\mathbf{c}(\tau')^H \mathbf{c}(\tau^0)}{\|\mathbf{c}(\tau')\| \, \|\mathbf{c}(\tau^0)\|} \, e^{j(\psi(\tau^0)-\psi(\tau'))} \right\}^2. \tag{94}$$

For small deviations $d\tau$ around τ_0, a first-order Taylor expansion yields

$$\psi(\tau^0) - \psi(\tau^0 + d\tau) \simeq -\left.\frac{\partial\psi(\tau)}{\partial\tau}\right|_{\tau^0} d\tau = \omega_c d\tau. \tag{95}$$

Therefore, the ambiguity function can be expressed as

$$\Xi(\tau';\tau^0) = \Xi_{bb}(\tau';\tau^0)\, \cos^2(\omega_c d\tau), \tag{96}$$

where the baseband ambiguity function is defined as

$$\Xi_{bb}(\tau';\tau^0) = (\alpha^0)^2 \left| \frac{\mathbf{c}(\tau')^{\mathrm{H}} \mathbf{c}(\tau^0)}{\|\mathbf{c}(\tau')\| \|\mathbf{c}(\tau^0)\|} \right|^2. \tag{97}$$

The complete ambiguity function consists of the baseband signal ambiguity function modulated by a cosine-squared function with frequency f_c. This creates a Dirac comb

sampling effect on the baseband ambiguity function, with the $\cos^2(\cdot)$ term forming a rapidly oscillating envelope with lobe spacing $\Delta\tau = \frac{\pi}{\omega_c} = \frac{1}{2f_c}$. For GPS L1 band ($f_c = 1575.42$ MHz), this yields approximately 0.32 nanoseconds between lobes, a fine structure that enables precise timing discrimination through carrier-phase information. Figure 2 illustrates that structure for such GPS L1 C/A code sequence, where the carrier frequency $\mathrm{F_c}$ directly determines the lobe spacing. The comparison between Figures 2a and 2b demonstrates the impact of carrier frequency scaling: the tenfold increase in $\mathrm{F_c}$ produces proportionally narrower lobes and denser spacing, with Figure 2b containing significantly more lobes despite covering a narrower delay range. For correct MLE identification of the main lobe, its amplitude difference against adjacent lobes must exceed the noise floor. This representation also provides an intuitive interpretation of the gap between the conventional CRB and the phase-aware CRB. As already observed in previous studies on ambiguity-function-based estimation analysis [28], the additional phase information effectively reduces the ambiguity level by improving the discrimination of the main lobe with respect to secondary lobes. Consequently, reliable MLE identification requires the amplitude difference between the principal lobe and adjacent lobes to remain above the noise floor.

9. Detailed analysis of the MLE function and origin of the plateau

Starting from the expression of the concentrated MLE cost function $S_2(\mathbf{x}, x_a; \varphi, \boldsymbol{\eta})$ given in Eq. (20), and using the definition of the output signal-to-noise ratio

$$\mathrm{SNR_{out}} = \frac{|\alpha^0|^2 \|\mathbf{a}(\boldsymbol{\eta}^0)\|^2}{\sigma_n^2},$$

the cost function can be rewritten (from Eq. (20) after normalizing the matched-filter output by $|\alpha^0|\,\|\mathbf{a}(\boldsymbol{\eta}^0)\|$ and expressing the noise variance through $\mathrm{SNR_{out}}$) as

$$S_a^2(\mathbf{x}, x_a; \varphi, \boldsymbol{\eta}) = \underbrace{\frac{(x_a - \varphi)^2}{2\,\mathrm{SNR_{out}}\sigma_{n_a}^2}}_{T_1} - \underbrace{\cos^2\!\left(\arg\!\left(\frac{\mathbf{a}(\boldsymbol{\eta})^H \mathbf{x}}{\|\mathbf{a}(\boldsymbol{\eta})\|}\right) - \varphi\right)}_{T_2} \underbrace{\left|\frac{\mathbf{a}(\boldsymbol{\eta})^H \mathbf{x}}{\|\mathbf{a}(\boldsymbol{\eta})\| |\alpha^0| \|\mathbf{a}(\boldsymbol{\eta}^0)\|}\right|^2}_{T_3}, \quad (98)$$

where the three terms T_1, T_2, and T_3 capture complementary mechanisms governing the MLE behavior.

9.1. Physical interpretation

The different terms can be interpreted as follows:

- T_1 represents the deterministic phase mismatch between the auxiliary phase observation x_a and the estimated phase φ. In ideal conditions, T_1 decreases with increasing SNR and vanishes as the phase estimate converges.
- $T_2 = \cos^2(\Delta\phi)$ quantifies how well the phase of the received signal aligns with the phase predicted by the model. Once synchronization is achieved, $T_2 \approx 1$, indicating nearly perfect phase alignment.
- T_3 corresponds to the normalized correlation power between the received signal and the assumed model. It increases monotonically with SNR and asymptotically approaches unity, reflecting full signal–model coherence.

9.2. Origin of the plateau

Figure 3 provides a joint visualization of those contributions. As the SNR increases, T_3 rapidly approaches unity, indicating that the signal is already well matched to the model. In contrast, T_2 does not immediately converge to one. Instead, it remains below unity over the SNR interval corresponding to the plateau, and only reaches values close to one at the SNR threshold where the plateau ends. This behavior indicates that phase alignment is not yet fully achieved within the plateau region. At the same time, T_1 exhibits a markedly different behavior: it decreases very rapidly toward zero over a finite SNR range. This indicates that the phase estimate $\hat{\varphi} = \hat{\varepsilon}+x_a$ (30), quickly reaches high accuracy, with its error becoming negligible as the SNR increases. As a result, the overall cost function ceases to evolve, producing the observed performance plateau. That phenomenon can be interpreted as a *phase-locking regime*, in which correlation is already achieved, but phase coherence is only partially established. Once T_2 approaches unity, corresponding to accurate phase compensation, the estimator exits this regime and resumes improving its performance with increasing SNR.

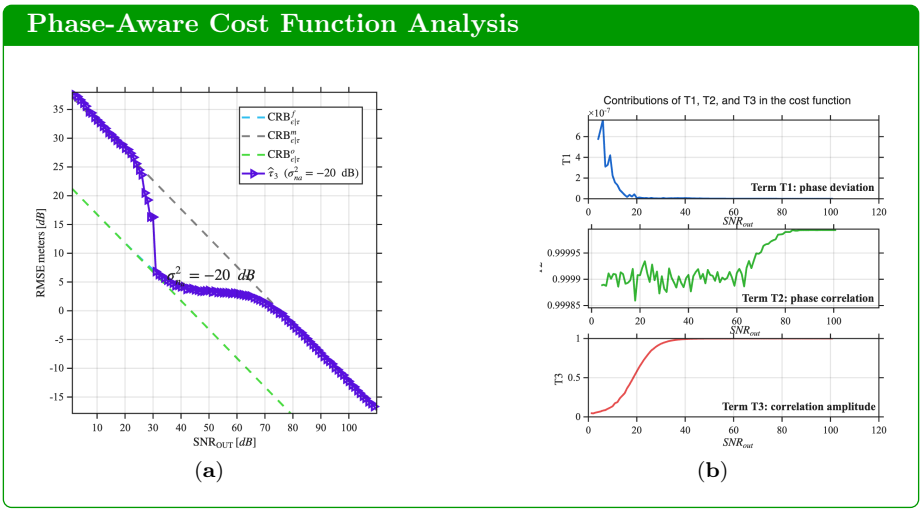


Figure 3: Decomposition of the phase-aware maximum-likelihood cost function, S_2, into its three components (T_1, T_2, and T_3) for the Kasami signal configuration.

9.3. Estimator behavior across SNR

At low SNR, the estimator is dominated by noise and $\hat{\tau}_3$ randomly jumps between secondary peaks of the ambiguity function 2b. As SNR increases, the estimator enters the plateau region, corresponding to the phase-locking regime identified above. In that region, $\hat{\tau}_3$ locks onto the main correlation peak but still exhibits small oscillations due to residual phase uncertainty. This phase is not fully resolved because of the finite variance of the auxiliary phase observation, $\sigma^2_{n_a}$. However, its relative impact progressively decreases with increasing SNR. Indeed, as $\sigma^2_n \to 0$, the weight of the phase regularization term becomes less significant compared to the correlation term, as already suggested by (74), (75). That behavior is consistent with the asymptotic covariance expression, where $\sigma^2_{n_a}$ appears normalized by σ^2_n, so that the influence of

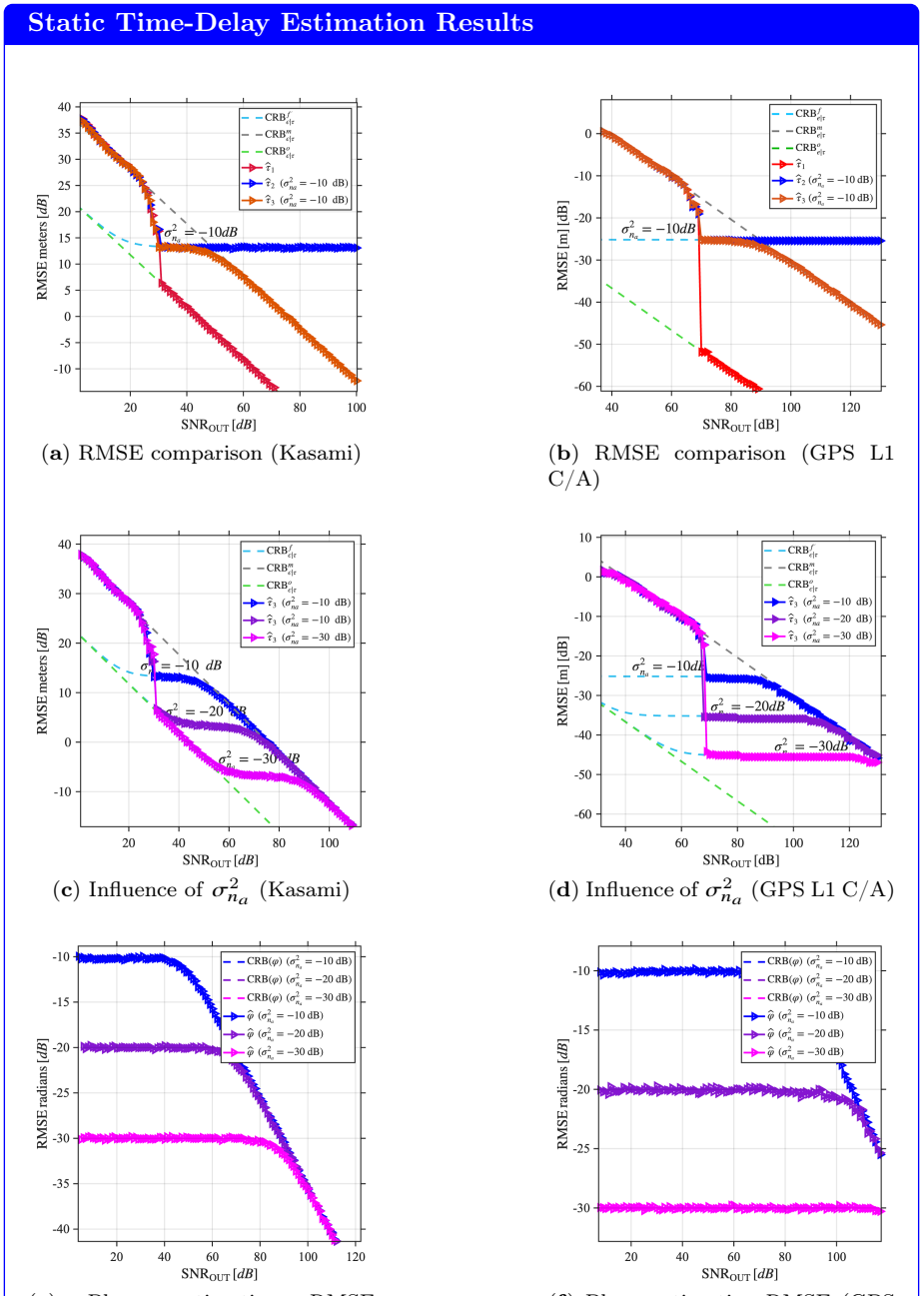
the phase noise vanishes as the observation noise decreases. Beyond that regime, the phase estimate progressively improves, T_1 reduces, and the estimator transitions to the asymptotic regime. The delay estimate then converges steadily to the true value, achieving stable and optimal performance.

10. Numerical simulations and discussion

This section validates the proposed framework through numerical simulations. The consistency between the derived CRBs and the MLEs is first assessed under the proposed CSM assumptions, following [20, 29]. Estimator performance is then evaluated under realistic conditions with fixed phase uncertainty $\sigma_{n_a}^2$. Unless otherwise stated, simulations consider the delay-only scenario and additional results including Doppler assess the impact of frequency offsets. Under realistic conditions, $\sigma_{n_a}^2$ is independent of SNR and reflects calibration uncertainty. In this case, three distinct regimes emerge. Before entering the asymptotic region, however, the MLE does not yet converge to either bound. In this transition regime, estimation performance is still affected by ambiguity effects and residual phase uncertainty, leading to a gap between the achieved RMSE and both CRB^m and CRB^f. As SNR increases, an intermediate regime appears in which the estimator exhibits a plateau. In that region, performance converges to CRB^f, and the plateau level scales linearly with $\sigma_{n_a}^2$, establishing a direct link between calibration quality and achievable accuracy. At high SNR, the phase-dependent contribution vanishes and CRB^f converges toward CRB^m. The estimator then relies solely on the baseband ambiguity function envelope, effectively losing the benefit of carrier-phase information. The performance of the optimal, naive, and phase-aware estimators is analyzed under fixed phase uncertainty conditions for both Kasami and GPS L1 C/A signal configurations. The comparison highlights the impact of residual phase uncertainty on the asymptotic estimation accuracy and illustrates the different operating regimes predicted by the derived CRB expressions.

10.0.1. Time-delay estimation only

A static scenario is considered with $b = v/c_e = 0$. Figures 4a–4b compare the RMSE performance of the optimal estimator $\widehat{\tau}_1$ ((88) with $\sigma_{na}^2 \to 0$), the naive estimator $\widehat{\tau}_2$ ((23) with $\boldsymbol{\eta} = \tau$), and the proposed phase-aware estimator $\widehat{\tau}_3$ ((88)) for Kasami and GPS L1 C/A signals under fixed phase uncertainty. Three operating regimes are observed. At low SNR, all estimators are significantly affected by thermal noise phenomena, and none of them achieves the corresponding CRB^m. At intermediate SNR, both $\widehat{\tau}_2$ and $\widehat{\tau}_3$ exhibit a plateau caused by residual phase uncertainty. The proposed phase-aware estimator eventually departs from the plateau and converges toward CRB^m, whereas the naive estimator remains saturation-limited. Figures 4c–4d analyze the impact of the phase-noise variance $\sigma_{n_a}^2$ on the proposed MLE.



(**a**) RMSE comparison (Kasami)

(**b**) RMSE comparison (GPS L1 C/A)

(**c**) Influence of $\sigma^2_{n_a}$ (Kasami)

(**d**) Influence of $\sigma^2_{n_a}$ (GPS L1 C/A)

(**e**) Phase estimation RMSE (Kasami)

(**f**) Phase estimation RMSE (GPS L1 C/A)

Figure 4: Static time-delay estimation results for Kasami and GPS L1/C/A signals. Comparison of the optimal, naive, and phase-aware estimators together with the impact of $\sigma^2_{n_a}$ and the corresponding phase estimation performance.

Reducing $\sigma_{n_a}^2$ lowers the plateau and extends the SNR region where carrier-phase information improves delay estimation accuracy. For sufficiently high SNR, all curves progressively converge toward CRB^m, confirming the asymptotic behavior predicted by the theoretical analysis. The high-SNR region is included only for validation purposes and does not represent typical operating conditions. Figures 4e–4f show the phase estimation performance for both signal configurations. The phase estimator $\hat{\varphi}$ (30) follows the predicted CRB and exhibits the same regime transition as the time-delay estimator. At intermediate SNR, the phase estimation error is dominated by the auxiliary phase uncertainty, while at high SNR the estimator asymptotically achieves the theoretical bound. These results experimentally validate the coupling between phase estimation and TDE predicted by the derived CRB expressions.

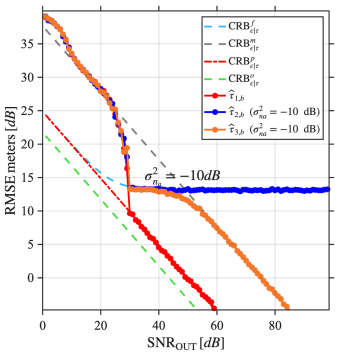
10.0.2. Time-delay and Doppler simulations

Here we set a low dynamic scenario and we set $b = v/c_e = 10^{-8}$. Figures 5a–5b extend the previous analysis to the joint delay-Doppler estimation scenario. The introduction of Doppler produces an additional coupling between parameters, which increases the estimation difficulty. Despite that increased coupling, the proposed phase-aware estimator $\hat{\tau}_{3,b}$ (31) preserves the same asymptotic behavior observed in the delay-only case. The optimal estimator $\hat{\tau}_{1,b}$ ((31) with $\sigma_{na}^2 \to 0$) still achieves the best overall performance, while the naive estimator $\hat{\tau}_{2,b}$ (23) remains limited by the phase-noise-induced plateau. All Cramér–Rao Bounds are represented by dashed curves. The red dashed curve corresponds to the ideal bound obtained under perfect phase knowledge, while the light-blue dashed curves represent the conditional bounds that accounts for phase uncertainty for the joint parameter vector $\boldsymbol{\eta} = [\tau, b]^T$. These bounds complement the previously introduced CRBs and provide the theoretical performance limits for the joint delay-Doppler estimation problem. Figures 5c–5d investigate the influence of $\sigma_{n_a}^2$ in the presence of Doppler. A similar performance plateau occurs in this scenario, though it shifts toward higher SNR values due to the additional uncertainty introduced by the Doppler effect. Reducing $\sigma_{n_a}^2$ again improves the achievable estimation accuracy and delays the onset of saturation effects. The agreement between Monte Carlo simulations and the theoretical CRB confirms the validity of the proposed asymptotic analysis in coupled delay-Doppler conditions. Figures 5e–5f present the RMSE of the Doppler estimate $\hat{b}_3$ associated with the proposed phase-aware estimator (31) together with the corresponding CRB, for a fixed phase-noise variance $\sigma_{n_a}^2 = -10$ dB. The estimator asymptotically approaches the theoretical bound for both signal configurations, confirming the consistency of the joint delay-Doppler estimation framework. The Doppler estimation accuracy improves with increasing SNR until reaching the phase-noise-limited region imposed by $\sigma_{n_a}^2$.

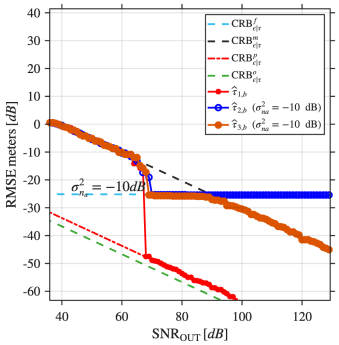
10.1. Practical implications

The results highlight a fundamental trade-off between SNR and phase calibration accuracy. Incorporating phase information significantly reduces the SNR required to achieve meter-level ranging accuracy. However, sub-centimeter precision requires both high SNR and accurate phase calibration. For the considered configurations, the GPS L1 C/A signal achieves centimeter-level accuracy only in the high-SNR regime, whereas shorter sequences such as Kasami remain limited to decimeter-level performance due to their reduced time-bandwidth product and lower carrier frequency. Overall, high-precision ranging requires the joint optimization of signal design, carrier frequency, sampling rate, sequence duration, and phase calibration.

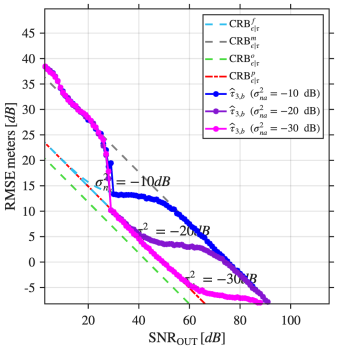
Joint Delay–Doppler Estimation Results



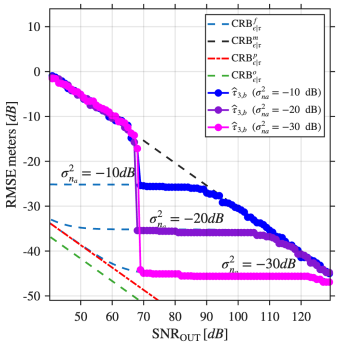
(**a**) RMSE comparison (Kasami)



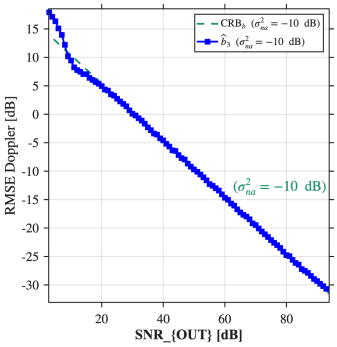
(**b**) RMSE comparison (GPS L1 C/A)



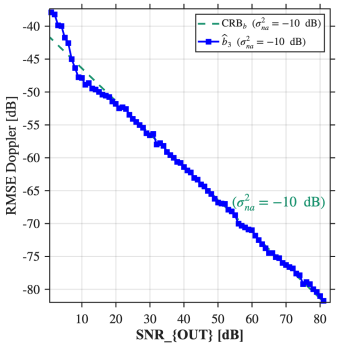
(**c**) Influence of $\sigma^2_{n_a}$ (Kasami)



(**d**) Influence of $\sigma^2_{n_a}$ (GPS L1 C/A)



(**e**) Doppler estimation RMSE (Kasami)



(**f**) Doppler estimation RMSE (GPS L1 C/A)

Figure 5: Joint delay–Doppler estimation results for Kasami and GPS L1/C/A signals. Comparison of the optimal, naive, and phase-aware estimators together with the influence of $\sigma^2_{n_a}$ and the corresponding Doppler RMSE/CRB.

11. Conclusion

This work investigated single source deterministic parameters estimation in the presence of hardware-induced phase offsets observed through uncertain auxiliary measurements. Within the CSM framework, identifiability conditions were established, showing that hardware-induced and propagation-induced phase components can be both estimated under non-collinearity of the baseband signals. That result provides the theoretical basis for incorporating imperfect phase information into the estimation process. Building on this foundation, CRB and MLE formulations were derived to explicitly account for phase uncertainty. The resulting phase-aware estimator remains computationally tractable while achieving asymptotic efficiency. Its performance was compared against both an ideal estimator with perfect phase knowledge and a naive approach that neglects phase prior model. The analysis reveals a continuous transition between two fundamental regimes. When phase calibration uncertainty is large, the estimation problem reduces to the conventional case where phase information provides no benefit. Conversely, in the limit of vanishing calibration uncertainty, the estimator approaches the ideal performance bound. A key finding of this work is the emergence of an intermediate plateau in the estimation error as a function of SNR under realistic conditions. That effect, overlooked in the open literature, is driven by the finite accuracy of phase calibration rather than noise or correlation limitations. The ambiguity function perspective provides further insight into that behavior. Phase uncertainty prevents reliable discrimination between closely spaced carrier-induced lobes, causing the estimator to lose sensitivity to fine-scale structure. Only when the phase is sufficiently well characterized does the estimator fully exploit the carrier information and converge toward the fundamental limits. Overall, this work establishes phase uncertainty as a fundamental limiting factor in phase-aided time-delay estimation. It also identifies the conditions under which modeling that uncertainty is beneficial, showing that phase-aware estimation provides tangible gains only beyond a critical SNR threshold. Those results highlight the need for joint optimization of signal design, SNR, and calibration accuracy to achieve high-precision ranging.

Acknowledgment

This work was partially supported by CNES, IPSA and DGA/AID project 2023.65.0083 and 2025.65.0026.

References

[1] E. D. Kaplan (Ed.), Understanding GPS: principles and applications, 2nd Edition, Artech House, 2006.

[2] M. I. Skolnik, Radar Handbook, 3rd Edition, McGraw-Hill, New York, USA, 1990. doi:https://doi.org/10.1109/MAES.2008.4523916.

[3] H. L. Van Trees, Optimum Array Processing, Wiley-Interscience, New York, 2002. doi:10.1002/0471221104.

[4] J. Chen, Y. Huang, J. Benesty, Time Delay Estimation, Springer US, Boston, MA, 2004, pp. 197–227. doi:10.1007/1-4020-7769-6_8.
URL https://doi.org/10.1007/1-4020-7769-6_8

[5] U. Mengali, A. N. D'Andrea, Synchronization Techniques for Digital Receivers, Applications of Communications Theory, Springer, 1997. doi:10.1007/978-1-4899-1807-9.

[6] D. Medina, L. Ortega, J. Vilà-Valls, P. Closas, F. Vincent, E. Chaumette, Compact CRB for delay, doppler and phase estimation - application to GNSS SPP & RTK performance characterization, IET Radar, Sonar & Navigation 14 (10) (2020) 1537–1549. doi:https://doi.org/10.1049/iet-rsn.2020.0168.

[7] P. Das, J. Vila-Valls, E. Chaumette, F. Vincent, L. Davain, S. Bonnabel, On the accuracy limit of time-delay estimation with a band-limited signal, in: Proceedings of the IEEE International Conference on Acoustics, Speech and Signal Processing (ICASSP), Brighton, UK, 2019, pp. 4330–4334. doi:10.1109/ICASSP.2019.8682592.

[8] C. Lubeigt, L. Ortega, J. Vilà-Valls, L. Lestarquit, E. Chaumette, Joint delay-doppler estimation performance in a dual source context, Remote Sensing 12 (23) (2020). doi:10.3390/rs12233894.

[9] S. F. Yau, Y. Bresler, A compact Cramér–Rao bound expression for parametric estimation of superimposed signals, IEEE Transactions on Signal Processing 40 (5) (1992) 1226–1230. doi:10.1109/78.134446.

[10] H. L. Van Trees, K. L. Bell, Z. Tian, Detection, Estimation, and Modulation Theory, Part I, 2nd Edition, Wiley, 2013. doi:10.1002/9781118391228.

[11] S. M. Kay, Fundamentals of Statistical Signal Processing: Estimation Theory, Prentice-Hall, Englewood Cliffs, New Jersey, USA, 1993.

[12] P. Stoica, A. Nehorai, Performances study of conditional and unconditional direction of arrival estimation, IEEE Trans. Acoust., Speech, Signal Process. 38 (10) (1990) 1783–1795. doi:https://doi.org/10.1109/29.60109.

[13] P. J. G. Teunissen, O. Montenbruck (Eds.), Handbook of Global Navigation Satellite Systems, Springer, Switzerland, 2017. doi:https://doi.org/10.1007/978-3-319-42928-1.

[14] N. Noels, H. Wymeersch, H. Steendam, M. Moeneclaey, True Cramér–Rao bound for timing recovery from a bandlimited linearly modulated waveform with unknown carrier phase and frequency, IEEE Transactions on Communications 52 (3) (2004) 473–483. doi:10.1109/TCOMM.2004.825751.

[15] H.-W. Wei, S. Ye, Q. Wan, Influence of random carrier phase on the true Cramér–Rao lower bound for time delay estimation, in: Proceedings of the IEEE International Conference on Acoustics, Speech and Signal Processing (ICASSP), Honolulu, HI, USA, 2007, pp. 1029–1032. doi:10.1109/ICASSP.2007.366858.

[16] H. L. Van Trees, Detection, Estimation, and Modulation Theory, Part III: Radar–Sonar Signal Processing and Gaussian Signals in Noise, John Wiley & Sons, 2001. doi:10.1002/0471221082.

[17] D. Slepian, Estimation of signal parameters in the presence of noise, Transactions of the IRE Professional Group on Information Theory 3 (3) (1954) 68–89. doi:10.1109/IREPGIT.1954.6373401.

[18] G. A. F. Seber, Matrix Handbook for Statisticians, Wiley Series in Probability and Statistics, 2008.

[19] P. Das, J. Vila-Valls, F. Vincent, L. Davain, E. Chaumette, A new compact delay, doppler stretch and phase estimation CRB with a band-limited signal for gene. remote sensing applications, Remote Sensing 12 (18) (2020) 2913. doi:10.3390/rs12182913.

[20] J. Bernabeu, L. Ortega, A. Blais, Y. Grégoire, E. Chaumette, Time-delay maximum-likelihood estimator under phase uncertainty, in: 2025 IEEE 10th International Workshop on Computational Advances in Multi-Sensor Adaptive Processing (CAMSAP), 2025. doi:https://doi.org/10.1109/HSCMA.2008.4538695.

[21] R. C. Davis, L. E. Brennan, I. S. Reed, Angle estimation with adaptive arrays in external noise fields, IEEE Transactions on Aerospace and Electronic Systems AES-12 (2) (1976) 179–186. doi:10.1109/TAES.1976.308293.

[22] M. R. Osborne, Fisher's method of scoring, International Statistical Review 60 (1992) 99–117.

[23] U. Nickel, Monopulse estimation with adaptive arrays, IEE Proceedings - Radar, Sonar and Navigation 140 (5) (1993) 303–308.

[24] T. J. Moore, B. M. Sadler, R. J. Kozick, Maximum-likelihood estimation, the cramér-rao bound, and the method of scoring with parameter constraints, IEEE Transactions on Signal Processing 56 (3) (2008) 895–908. doi:10.1109/TSP.2007.907814.

[25] J. Bernabeu, S. Alteri, A. Blais, L. Ortega, Y. Grégoire, É. Chaumette, Technical note on asymptotic covariance derivation, Tech. rep., ISAE-SUPAERO, Toulouse, France, technical note accompanying "Revisiting the Conditional Single Signal Model with Phase Uncertainty: Application to Time-Delay Estimation" (2025). doi:https://doi.org/10.13140/RG.2.2.23818.84165.

[26] B. Ottersten, M. Viberg, P. Stoica, A. Nehorai, Exact and Large Sample Maximum Likelihood Techniques for Parameter Estimation and Detection in Array Processing, in: S. Haykin, J. Litva, T. J. Shepherd (Eds.), Radar Array Processing, Springer-Verlag, Heidelberg, 1993, Ch. 4, pp. 99–151.

[27] J. K. Holmes, Spread spectrum systems for GNSS and wireless communications, Artech House Norwood, MA, 2007.

[28] J. Bernabeu, L. Ortega, E. Chaumette, Revisiting the conditional signal model for time-delay estimation analysis, EURASIP Journal on Advances in Signal Processing 2024 (1) (2024) 1–18. doi:10.1186/s13634-024-01142-4.

[29] A. Renaux, P. Forster, E. Chaumette, P. Larzabal, On the high-SNR conditional maximum-likelihood estimator full statistical characterization, IEEE Trans. Signal Process. 54 (12) (2006) 4840 – 4843. doi:https://doi.org/10.1109/TSP.2006.882072.